Electronic Supplementary Information (ESI) for Chemical Science

Supporting Information

Isomeric Model Molecules: Understanding and Regulating the Emission Nature of Multiple-Resonance Thermally Activated Delayed Fluorescence

Xinliang Cai,[#,a,b] Rajat Walia,[#,c] Weixiong Guo,[d] Yexuan Pu,[b] Jinbei Wei,[*,a] Xian-Kai Chen,[*,c] and Yue Wang[*,b]

[a]State Key Laboratory of Integrated Optoelectronics, JLU Region, College of Electronic Science and Engineering, Jilin University, Changchun 130012, P. R. China
E-mail: jinbwei@jlu.edu.cn
[b]State Key Laboratory of Supramolecular Structure and Materials College of Chemistry, Jilin University, Changchun 130012, P. R. China
E-mail: yuewang@jlu.edu.cn
[c]Institute of Functional Nano and Soft Materials (FUNSOM), Joint International Research Laboratory of Carbon-Based Functional Materials and Devices, Soochow University, Suzhou, Jiangsu, P. R. China.
E-mail: xkchen@suda.edu.cn
[d]Department of Chemistry, City University of Hong Kong, Kowloon, Hong Kong SAR, P. R. China.

Table of Contents for Supporing Information

1. General Information

Thermo Fisher ITQ1100 GC/MS and Kratos AXIMA-CFR Kompact MALDI mass spectrometer were employed to measure the mass spectra. High resolution mass spectra were recorded on a Bruker Solarix FT-ICR mass spectrometer. Flash EA 1112 spectrometer was used to perform the elemental analyses. Bruker AVANCE III 400, 500 MHz and 600 MHz were selected to measure the ^{1}H and ^{13}C spectra with tetramethylsilane (TMS) as the internal standard. BOF-5-50 vacuum sublimation instrument (AnHui BEQ Equipment Technology CO., Ltd) was used to sublimate the target compound. Edinburgh FLS1000 and Shimadzu UV-2550 spectrophotometer were adopted to record the Photoluminescence (PL) emission spectra and UV-Vis absorption, respectively. The fluorescence and phosphorescent spectra taken at liquid nitrogen temperature (77 K) were recorded by Ocean Optics QE Pro with a 365 nm Ocean Optics LLS excitation source. Edinburgh FLS920 steady state fluorimeter equipping with an integrating sphere was employed to measure the absolute fluorescence quantum yields of both solutions and films at room temperature. FLS1000 fluorescence lifetime measurement system with 365 nm LED excitation source was selected to investigate the transient PL decay and temperature-dependent transient PL decay of solid films. TA Q500 thermogravimeter was selected to perform the thermogravimetric analysis (TGA) of target molecules under nitrogen atmosphere at a heating rate of 10 K min $^{-1}$. BAS 100W Bioanalytical electrochemical work station was used to measure the electrochemical property with platinum disk as working electrode, platinum wire as auxiliary electrode, a porous glass wick Ag/Ag^{+} as pseudo reference electrode and ferrocene/ferrocenium as the internal standard. And 0.1 M solution of *n*-Bu_4NPF_6 which was the supporting electrolyte was utilized to measure the oxidation and reduction potentials (in anhydrous CH_2Cl_2 and DMF, respectively) at a scan rate of 100 mV s $^{-1}$.

2. Theoretical calculation

The ground-state geometries of all molecules were optimized using the empirically tuned ω parameter in the ωB97XD functional within the Gaussian 16 package[S1]. Based on these optimized geometries, all one- and two-electron integrals were computed at the Hartree-Fock level using the PySCF quantum chemistry program[S2]. Excited-state calculations were then performed using the configurational interaction singles (CIS) and similarity-transformed equation-of-motion coupled-cluster method with domain-based local pair natural orbitals (STEOM-DLPNO-CCSD) as implemented in ORCA 4.2.1[S3]. Percentage atomic contributions to the HOMO and LUMO were calculated using Mulliken-partition analysis in Multiwfn based on restricted Hartree-Fock orbitals[S4]. The def2-TZVP basis set was used in all calculations.

In this work, the following energies were defined for the S_1 states of all molecules:

(1) $\boldsymbol{E_{S1}}$**[CIS]** – the S_1 energy obtained from configuration interaction singles (CIS) calculations, which lacks the inclusion of correlation effects in excited states.

(2) $\boldsymbol{E_{S1}}$**[CC]** – the S_1 energy obtained from STEOM-DLPNO-CCSD calculations, which include electron correlation effects.

(3) $\boldsymbol{E_{S1}}$**[Ints]** – the S_1 energy estimated solely from one- and two-electron integrals within a two-electron two-orbital (HOMO-LUMO) framework. In this model, the ground-state energy is given by,

$$E_{S0} = 2h_{HH} + J_{HH}$$

and the S_1-state energy is,

$$E_{S1} = h_{HH} + h_{LL} + J_{HL} + K_{HL}$$

where h_{ii} are the one-electron integrals and J_{HL}, K_{HL} are the Coulombic and exchange integrals between HOMO and LUMO. The S_1 excitation energy from integrals is then defined as

$$E_{S1}[\text{Ints}] = E_{S1} - E_{S0}$$

(4) $\boldsymbol{E_{S1}}$**[Corr]** – the electron correlation contribution, obtained as the difference between the CC- and CIS-calculated S_1 energies:

$$E_{S1}[\text{Corr}] = E_{S1}[\text{CC}] - E_{S1}[\text{CIS}]$$

Since CIS energies are systematically overestimated, the E_{S1}[Corr] is always negative, reflecting the stabilizing effect of electron correlation on the S_1 state. This arises because CIS neglects electron correlation, whereas STEOM-DLPNO-CCSD accounts for it. Thus, the difference between the two energies directly quantifies the electron-correlation stabilization in S_1 state.

(5) $\boldsymbol{E_{S1}}$**[Ints+Corr]** – the S_1 energy incorporating both integral and correlation effects:

$$E_{S1}[\text{Corr}] = E_{S1}[\text{Ints}] + E_{S1}[\text{Corr}]$$

This framework allows the separate analysis of contributions from basic integrals and electron correlation to the S_1 excitation energy.

3. Synthesis of Materials

All reagents were purchased from *Energy Chemical Co.* and/or *J&K Scientific Ltd. Co.* and immediately used without further purification. Schlenk technology was strictly performed under nitrogen conditions in all reactions. The detailed synthesis procedures are described below.

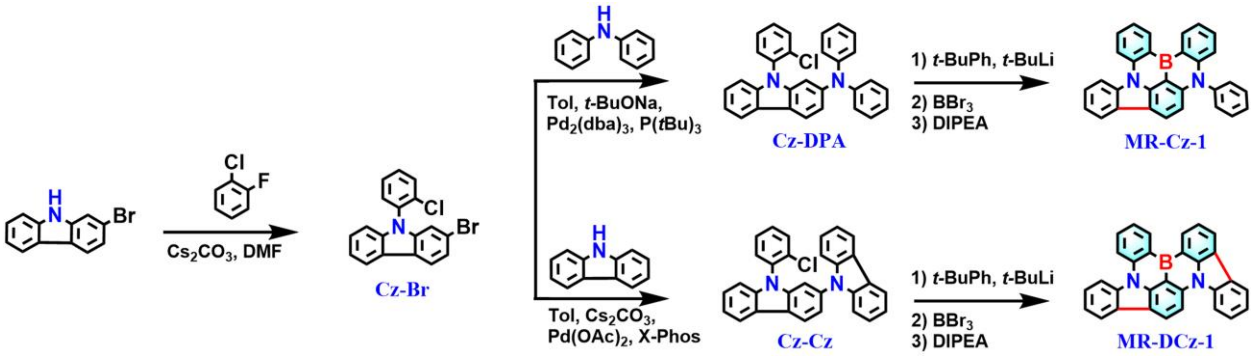

Scheme S1. Synthetic procedures of MR-Cz-1 and MR-DCz-1.

Synthesis of Cz-Br: 2-bromo-9*H*-carbazole (27.1 g, 110.0 mmol), Cs_2CO_3 (48.9 g, 150.0 mmol) and 1-chloro-2-fluorobenzene (13.1 g, 100.0 mmol) were dissolved in *N*, *N*-dimethylformamide (DMF, 200 mL). The mixture was stirred at 150 ºC for 24 h under nitrogen. After cooling to room temperature, the resulting product was diluted with chloroform and washed with water. The combined organic extracts were dried over Na_2SO_4 and concentrated under reduced pressure. The crude product was purified by column chromatography with dichloromethane/petroleum (1: 9) as eluent to afford Cz-Br as a colorless oil (yield = 33.5 g, 94%). ^{1}H NMR (500 MHz, DMSO-d_6) δ 8.26 (dd, *J* = 22.8, 8.0 Hz, 2H), 7.86 (dd, *J* = 7.6, 1.8 Hz, 1H), 7.69 (dqd, *J* = 14.6, 7.3, 2.0 Hz, 3H), 7.50-7.42 (m, 2H), 7.33 (t, *J* = 7.5 Hz, 1H), 7.16 (d, *J* = 1.7 Hz, 1H), 7.04 (d, *J* = 8.2 Hz, 1H). ^{13}C NMR (151 MHz, $CDCl_3$) δ 141.70, 141.11, 134.44, 133.75, 131.24, 130.83, 130.28, 128.34, 126.50, 123.32, 122.77, 122.37, 121.61, 120.61, 120.42, 119.63, 113.08, 110.25. MALDI-TOF MS: m/z: 355.12 [M]+ (calcd: 354.98). Anal. Calcd for $C_{18}H_{11}BrClN$: C, 60.62; H, 3.11; Br, 22.40; Cl, 9.94; N, 3.93. Found: C, 60.58; H, 3.12; N, 3.97.

Synthesis of Cz-DPA: Cz-Br (14.3 g, 40.0 mmol), *t*-BuONa (7.7 g, 80.0 mmol), diphenylamine (7.8 g, 46.0 mmol), $Pd_2(dba)_3$ (0.9 g, 1.0 mmol) and $P(tBu)_3$ (0.4 g, 2.0 mmol) were dissolved in toluene (Tol, 150 mL). The mixture was stirred at 110 ºC for 24 h under nitrogen. After cooling to room temperature, the resulting product was diluted with chloroform and washed with water.

The combined organic extracts were dried over Na_2SO_4 and concentrated under reduced pressure. The crude product was purified by column chromatography with dichloromethane/petroleum (1: 6) as eluent to afford Cz-DPA as a white solid (yield = 16.4 g, 92%). ^{1}H NMR (500 MHz, DMSO-d_6) δ 8.14 (dd, *J* = 8.1, 4.4 Hz, 2H), 7.80-7.69 (m, 1H), 7.63 (dt, *J* = 7.5, 3.7 Hz, 1H), 7.60-7.53 (m, 2H), 7.35 (ddd, *J* = 8.4, 7.2, 1.2 Hz, 1H), 7.26 (td, *J* = 8.0, 7.2, 2.0 Hz, 5H), 7.07-6.95 (m, 7H), 6.92 (dd, *J* = 8.4, 2.0 Hz, 1H), 6.61 (d, *J* = 1.9 Hz, 1H). ^{13}C NMR (151 MHz, $CDCl_3$) δ 148.07, 146.28, 141.81, 141.32, 134.81, 133.47, 131.10, 130.61, 129.70, 129.06, 128.04, 125.24, 123.63, 123.32, 122.28, 120.96, 120.21, 119.76, 119.33, 118.54, 109.78, 106.59. MALDI-TOF MS: m/z: 443.91 [M]+ (calcd: 444.14). Anal. Calcd for $C_{30}H_{21}ClN_2$: C, 80.98; H, 4.76; Cl, 7.97; N, 6.30. Found: C, 81.02; H, 4.74; N, 6.27.

Synthesis of Cz-Cz: Cz-Br (14.3 g, 40.0 mmol), Cs_2CO_3 (26.1 g, 80.0 mmol), 9*H*-carbazole (7.7 g, 46.0 mmol), $Pd(OAc)_2$ (0.5 g, 2.0 mmol) and X-Phos (0.4 g, 3.0 mmol) were dissolved in Tol (150 mL). The mixture was stirred at 110 ºC for 24 h under nitrogen. After cooling to room temperature, the resulting product was diluted with chloroform and washed with water. The combined organic extracts were dried over Na_2SO_4 and concentrated under reduced pressure. The crude product was purified by column chromatography with dichloromethane/petroleum (1: 5) as eluent to afford Cz-Cz as a white solid (yield = 14.9 g, 84%). ^{1}H NMR (600 MHz, DMSO-d_6) δ 8.55 (d, *J* = 8.1 Hz, 1H), 8.39 (d, *J* = 7.7 Hz, 1H), 8.25 (d, *J* = 7.8 Hz, 2H), 7.86-7.76 (m, 2H), 7.64-7.59 (m, 2H), 7.53 (dd, *J* = 8.2, 1.8 Hz, 1H), 7.50 (ddd, *J* = 8.3, 7.2, 1.2 Hz, 1H), 7.46- 7.37 (m, 5H), 7.28 (ddd, *J* = 7.9, 6.0, 2.0 Hz, 2H), 7.19 (d, *J* = 1.7 Hz, 1H), 7.13 (d, *J* = 8.1 Hz, 1H). ^{13}C NMR (151 MHz, DMSO-d_6) δ 141.05, 140.85, 140.36, 134.83, 133.38, 132.02, 130.98, 130.93, 130.83, 129.05, 126.67, 126.18, 122.59, 122.22, 122.07, 121.94, 120.79, 120.58, 120.47, 119.94, 118.79, 109.82, 109.48, 107.88. MALDI-TOF MS: m/z: 442.34 [M]+ (calcd: 442.12). Anal. Calcd for $C_{30}H_{19}ClN_2$: C, 81.35; H, 4.32; Cl, 8.00; N, 6.32. Found: C, 81.33; H, 4.36; N, 6.28.

Synthesis of MR-Cz-1: The solution of *tert*-butyllithium in pentane (*t*-BuLi, 46.2 mL, 1.30 M, 60.0 mmol) was added slowly to a solution of Cz-DPA (13.3 g, 30.0 mmol) in *tert*-butylbenzene (*t*-BuPh, 150 mL) at 0 ºC under nitrogen atmosphere. After stirring at 70 ºC for 6 h, pentane was distilled at 70 °C. After addition of boron tribromide (BBr_3, 15.0 g, 60.0 mmol) at -30 ºC, the reaction mixture was stirred at room temperature for 6 h. *N*,*N*-diisopropylethylamine (DIPEA,

15.5 g, 120.0 mmol) was added at 0 ºC and then the reaction mixture was stirred at 150 ºC for 24 h. The resulted solution was extracted with dichloromethane/water, and the organic layer was concentrated in vacuum. The crude product was purified by column chromatography with dichloromethane/petroleum (1: 6) as eluent to afford MR-Cz-1 as a yellow solid (yield = 502.1 mg, 4%). ^{1}H NMR (400 MHz, DMSO-d_6) δ 9.28 (d, *J* = 7.8 Hz, 1H), 9.18 (d, *J* = 7.9 Hz, 1H), 9.01 (d, *J* = 8.6 Hz, 1H), 8.82 (d, *J* = 8.5 Hz, 1H), 8.57 (d, *J* = 8.7 Hz, 1H), 8.38 (d, *J* = 7.7 Hz, 1H), 8.07-7.98 (m, 1H), 7.87 (t, *J* = 7.7 Hz, 2H), 7.78 (t, *J* = 7.5 Hz, 1H), 7.72-7.62 (m, 3H), 7.59-7.51 (m, 3H), 7.47 (t, *J* = 7.4 Hz, 1H), 7.01 (d, *J* = 8.7 Hz, 1H), 6.68 (d, *J* = 8.7 Hz, 1H). ^{13}C NMR (151 MHz, $CDCl_3$) δ 147.51, 145.02, 144.19, 141.97, 140.27, 138.71, 136.57, 134.40, 131.29, 131.07, 130.90, 130.32, 128.93, 126.70, 124.79, 124.41, 122.19, 121.88, 120.26, 119.93, 118.25, 116.60, 114.66, 112.14, 108.15. MALDI: m/z: 418.29 [M]+ (calcd:418.16). Anal. Calcd for $C_{30}H_{19}BN_2$: C, 86.14; H, 4.58; B, 2.58; N, 6.70. Found: C, 86.13; H, 4.60; N, 2.55.

Synthesis of MR-DCz-1: MR-DCz-1 was synthesized according to the synthetic procedure of MR-Cz-1. The crude product was purified by column chromatography with dichloromethane/petroleum (1: 6) as eluent to afford MR-Cz-1 as a yellow solid (yield = 624.4 mg, 5%). ^{1}H NMR (500 MHz, $CDCl_3$) δ 9.14 (s, 1H), 8.94 (s, 1H), 8.71 (s, 1H), 8.50 (s, 2H), 8.46 (s, 1H), 8.39 (s, 2H), 8.23 (s, 2H), 7.86 (s, 1H), 7.69 (s, 1H), 7.60 (s, 2H), 7.49 (s, 3H). ^{13}C NMR (126 MHz, $C_2D_2Cl_4$) δ 143.67, 142.64, 140.91, 140.75, 139.73, 139.15, 137.18, 132.72, 132.28, 128.44, 127.35, 126.97, 126.29, 125.71, 125.37, 124.26, 123.39, 122.78, 122.50, 122.32, 121.00, 120.57, 116.46, 115.29, 114.76, 114.61, 107.37. MALDI: m/z: 416.29 [M]+ (calcd:416.15). Anal. Calcd for $C_{30}H_{17}BN_2$: C, 86.56; H, 4.12; B, 2.60; N, 6.73. Found: C, 86.59; H, 4.12; N, 6.74.

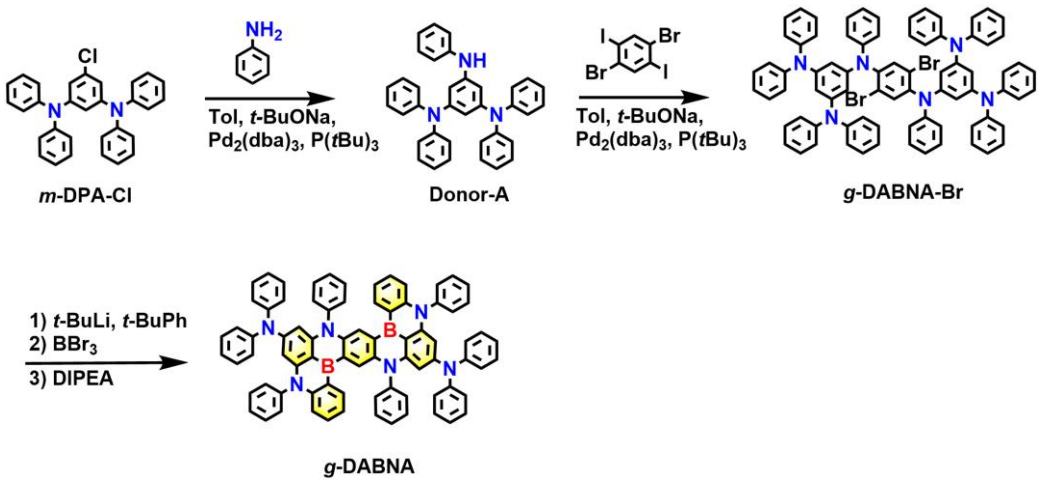

Scheme S2. Synthetic procedures of *g*-DABNA.

Synthesis of *m*-DPA-Cl: The synthetic process was referred to the reported literature.

Synthesis of Donor-A: *m*-DPA-Cl (44.7 g, 100.0 mmol), *t*-BuONa (17.3 g, 180.0 mmol), aniline (14.0 g, 150.0 mmol), $Pd_2(dba)_3$ (0.9 g, 1.0 mmol) and $P(tBu)_3$ (0.4 g, 2.0 mmol) were dissolved in Tol (300 mL). The mixture was stirred at 110 ºC for 24 h under nitrogen. After cooling to room temperature, the resulting product was diluted with chloroform and washed with water. The combined organic extracts were dried over Na_2SO_4 and concentrated under reduced pressure. The crude product was purified by column chromatography with dichloromethane/petroleum (1: 4) as eluent to afford Donor-A as a white solid (yield = 44.3 g, 88%). ^{1}H NMR (600 MHz, CD_2Cl_2) δ 7.22 (t, *J* = 7.8 Hz, 8H), 7.09 (dd, *J* = 17.0, 7.8 Hz, 10H), 6.97 (t, *J* = 7.4 Hz, 4H), 6.88 (d, *J* = 7.9 Hz, 2H), 6.33 (s, 3H). ^{13}C NMR (151 MHz, $CDCl_3$) δ 149.43, 147.50, 144.18, 142.69, 129.22, 129.14, 124.33, 122.78, 120.75, 117.32, 112.34, 107.70. MALDI-TOF MS: m/z: 503.64 [M]+ (calcd: 503.24). Anal. Calcd for $C_{36}H_{29}N_3$: C, 85.85; H, 5.80; N, 8.34. Found: C, 85.88; H, 5.81; N, 8.36.

Synthesis of *g*-DABNA-Br: Donor-A (6.0 g, 12.0 mmol), *t*-BuONa (3.4 g, 35.0 mmol), 1,4-dibromo-2,5-diiodobenzene (2.4 g, 5.0 mmol), $Pd_2(dba)_3$ (0.5 g, 0.5 mmol) and $P(tBu)_3$ (0.2 g, 1.0 mmol) were dissolved in Tol (40 mL). The mixture was stirred at 110 ºC for 24 h under nitrogen. After cooling to room temperature, the resulting product was diluted with chloroform and washed with water. The combined organic extracts were dried over Na_2SO_4 and concentrated under reduced pressure. The crude product was purified by column chromatography with dichloromethane/petroleum (1: 3) as eluent to afford *g*-DABNA-Br as a white solid (yield = 4.6 g,

74%). ^{1}H NMR (600 MHz, CD_2Cl_2) δ 7.23 (t, *J* = 7.8 Hz, 16H), 7.19 (t, *J* = 7.7 Hz, 4H), 7.08 (d, *J* = 8.0 Hz, 16H), 6.98 (t, *J* = 7.4 Hz, 10H), 6.83 (d, *J* = 8.0 Hz, 4H), 6.37 (s, 2H), 6.26 (s, 4H). ^{13}C NMR (151 MHz, CD_2Cl_2) δ 149.11, 147.80, 147.22, 143.50, 135.44, 129.00, 124.06, 122.74, 122.52, 122.38, 121.94, 113.39, 111.81. MALDI-TOF MS: m/z: 1238.59 [M]+ (calcd: 1238.31). Anal. Calcd for $C_{78}H_{58}Br_2N_6$: C, 75.60; H, 4.72; Br, 12.90; N, 6.78. Found: C, 75.58; H, 4.71; N, 6.76.

Synthesis of *g*-DABNA: The solution of *t*-BuLi in pentane (9.2 mL, 1.30 M, 12.0 mmol) was added slowly to a solution of *g*-DABNA-Br (3.7 g, 3.0 mmol) in *t*-BuPh (150 mL) at 0 ºC under nitrogen atmosphere. After stirring at 30 ºC for 2 h. After addition of BBr_3 (4.5 g, 18.0 mmol) at -30 ºC, the reaction mixture was stirred at room temperature for 6 h. DIPEA (3.9 g, 30.0 mmol) was added at 0 ºC and then the reaction mixture was stirred at 150 ºC for 24 h. The resulted solution was extracted with dichloromethane/water, and the organic layer was concentrated in vacuum. The crude product was dissolved in *o*-dichlorobenzene and then filtered with a pad of Florisil®. After the solvent was removed in vacuo, the crude product was purified by recrystallization from *o*-dichlorobenzene, resulting in an orange solid (yield = 1.1 g, 33%). Satisfactory NMR characterization (^{1}H and ^{13}C) could not be obtained for *g*-DABNA due to its extremely poor solubility in all conventional deuterated solvents. Therefore, high-resolution mass spectrometry (HRMS) were employed as alternative characterization methods for this compound. HRMS (MALDI-FTICR): m/z: 1096.4581 [M]+ (calcd:1096.4613). Anal. Calcd for $C_{78}H_{54}B_2N_6$: C, 85.41; H, 4.96; B, 1.97; N, 7.66. Found: C, 85.40; H, 4.96; N, 7.65.

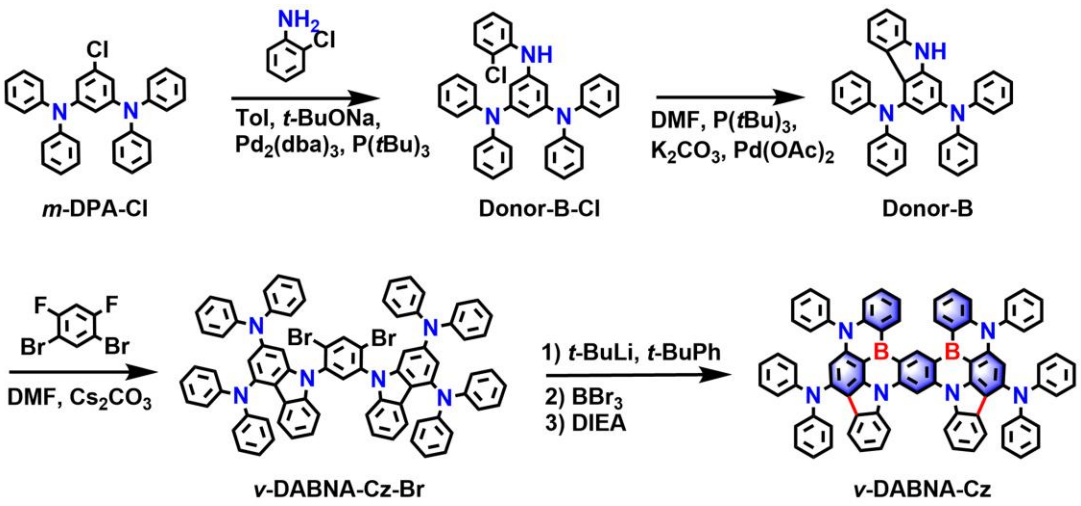

Scheme S3. Synthetic procedures of *v*-DABNA-Cz.

Synthesis of Donor-B-Cl: Donor-B-Cl was synthesized by replacing aniline with 2-chloroaniline according to the synthetic procedure of Donor-A. The crude product was purified by column chromatography with dichloromethane/petroleum (1: 5) as eluent to afford Donor-B-Cl as a white solid (yield = 24.8 g, 46%). ^{1}H NMR (600 MHz, DMSO-d_6) δ 7.71 (s, 1H), 7.31 (dd, *J* = 7.9, 1.6 Hz, 1H), 7.29 – 7.23 (m, 8H), 7.13 (dd, *J* = 8.2, 1.5 Hz, 1H), 7.06-7.02 (m, 9H), 6.98 (t, *J* = 7.4 Hz, 4H), 6.81 (td, *J* = 7.6, 1.5 Hz, 1H), 6.31 (d, *J* = 1.9 Hz, 2H), 6.13 (t, *J* = 2.0 Hz, 1H). ^{13}C NMR (151 MHz, DMSO-d_6) δ 148.45, 146.75, 144.49, 139.52, 129.84, 129.24, 127.19, 124.79, 124.00, 122.83, 121.74, 119.27, 109.89, 106.52. MALDI: m/z: 536.92 [M]+ (calcd:537.20). Anal. Calcd for $C_{36}H_{28}ClN_3$: C, 80.36; H, 5.25; Cl, 6.59; N, 7.81. Found: C, 80.32; H, 5.22; N, 7.83.

Synthesis of Donor-B: Donor-B-Cl (21.5 g, 40.0 mmol), K_2CO_3 (11.1 g, 80.0 mmol), $Pd(OAc)_2$ (0.5 g, 2.0 mmol) and P(tBu)$_3$ (0.8 g, 4.0 mmol) were dissolved in DMF (150 mL). The mixture was stirred at 150 ºC for 12 h under nitrogen. After cooling to room temperature, the resulting product was diluted with chloroform and washed with water. The combined organic extracts were dried over Na_2SO_4 and concentrated under reduced pressure. The crude product was purified by column chromatography with dichloromethane/petroleum (1: 3) as eluent to afford Donor-B as a white solid (yield = 18.3 g, 91%). ^{1}H NMR (600 MHz, DMSO-d_6) δ 11.21 (s, 1H), 7.37 (dd, *J* = 14.3, 8.0 Hz, 2H), 7.27-7.18 (m, 9H), 7.06-6.98 (m, 10H), 6.94-6.88 (m, 3H), 6.81 (t, *J* = 7.6 Hz, 1H), 6.52 (d, *J* = 1.9 Hz, 1H). ^{13}C NMR (151 MHz, $CDCl_3$) δ 147.78, 147.27, 147.09, 142.10, 141.67, 139.55, 129.13, 129.06, 124.84, 124.09, 122.68, 122.33, 121.79, 121.74, 119.64, 117.81,

116.14, 109.72, 103.41. MALDI-TOF MS: m/z: 500.96 [M]+ (calcd: 501.22). Anal. Calcd for $C_{36}H_{27}N_3$: C, 86.20; H, 5.43; N, 8.38. Found: C, 86.24; H, 5.40; N, 8.40.

Synthesis of *v*-DABNA-Cz-Br: Donor-B (5.5 g, 11.0 mmol), Cs_2CO_3 (6.5 g, 20.0 mmol) and 1,5-dibromo-2,4-difluorobenzene (1.4 g, 5.0 mmol) were dissolved in DMF (60 mL). The mixture was stirred at 150 ºC for 12 h under nitrogen. After cooling to room temperature, the resulting product was diluted with chloroform and washed with water. The combined organic extracts were dried over Na_2SO_4 and concentrated under reduced pressure. The crude product was purified by column chromatography with dichloromethane/petroleum (1: 3) as eluent to afford *v*-DABNA-Cz-Br as a white solid (yield = 5.1 g, 83%). ^{1}H NMR (600 MHz, CD_2Cl_2) δ 8.14 (s, 1H), 7.50 (s, 2H), 7.12 (d, *J* = 6.8 Hz, 8H), 7.08-7.03 (m, 10H), 7.03-7.00 (m, 10H), 6.97 (d, *J* = 8.0 Hz, 8H), 6.90 (d, *J* = 7.8 Hz, 2H), 6.86-6.83 (m, 8H), 6.73 (d, *J* = 8.2 Hz, 2H), 6.64 (dd, *J* = 4.7, 1.9 Hz, 2H), 6.60 (s, 1H). ^{13}C NMR (151 MHz, CD_2Cl_2) δ 147.45, 147.23, 141.90, 139.10, 137.28, 132.78, 129.08, 125.19, 124.44, 124.04, 123.86, 122.89, 122.80, 122.19, 121.93, 121.81, 121.78, 120.54, 118.42, 109.13. MALDI-TOF MS: m/z: 1235.02 [M]+ (calcd: 1234.28). Anal. Calcd for $C_{78}H_{54}Br_2N_6$: C, 75.85; H, 4.41; Br, 12.94; N, 6.80. Found: C, 75.88; H, 4.42; N, 6.77.

Synthesis of *v*-DABNA-Cz: *v*-DABNA-Cz was synthesized by replacing *g*-DABNA-Br with *v*-DABNA-Cz-Br according to the synthetic procedure of *g*-DABNA. The crude product was purified by column chromatography with dichloromethane/petroleum (1: 2) as eluent to afford *v*-DABNA-Cz as a yellow solid (yield = 1.0 g, 31%). ^{1}H NMR (600 MHz, CD_2Cl_2) δ 11.04 (s, 1H), 10.11 (s, 1H), 9.49 (d, *J* = 7.6 Hz, 2H), 8.84 (d, *J* = 8.4 Hz, 2H), 7.59 (d, *J* = 7.8 Hz, 2H), 7.52 (dd, *J* = 14.9, 7.5 Hz, 8H), 7.47 (d, *J* = 7.4 Hz, 4H), 7.44 (d, *J* = 7.6 Hz, 2H), 7.23 (d, *J* = 7.0 Hz, 4H), 7.16 (d, *J* = 7.2 Hz, 2H), 7.12 (d, *J* = 7.8 Hz, 8H), 7.02 (d, *J* = 8.0 Hz, 8H), 6.92 (t, *J* = 7.5 Hz, 4H), 6.20 (s, 2H). ^{13}C NMR data for *v*-DABNA-Cz could not be obtained due to its poor solubility in all conventional deuterated solvents. HRMS (MALDI-FTICR): m/z: 1092.4275 [M]+ (calcd:1092.4300). Anal. Calcd for $C_{78}H_{50}B_2N_6$: C, 85.72; H, 4.61; B, 1.98; N, 7.69. Found: C, 85.70; H, 4.63; N, 7.70.

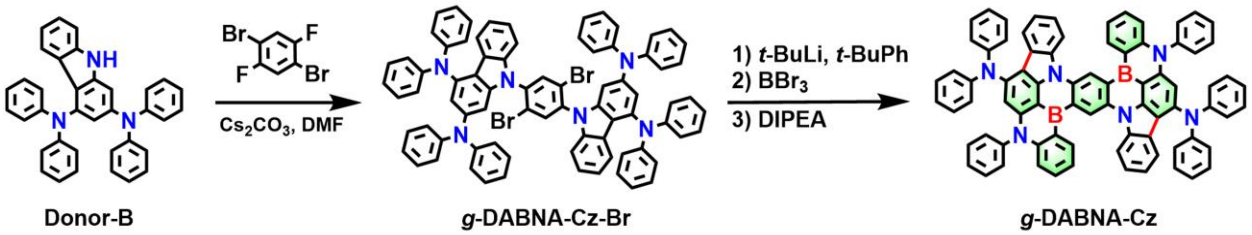

Scheme S4. Synthetic procedures of *g*-DABNA-Cz.

Synthesis of *g*-DABNA-Cz-Br: *g*-DABNA-Cz-Br was synthesized by replacing 1,5-dibromo-2,4-difluorobenzene with 1,4-dibromo-2,5-difluorobenzene according to the synthetic procedure of *v*-DABNA-Cz-Br. The crude product was purified by column chromatography with dichloromethane/petroleum (1: 2) as eluent to afford *g*-DABNA-Cz-Br as a light yellow solid (yield = 4.9 g, 80%). ^{1}H NMR (500 MHz, $C_2D_2Cl_4$) δ 7.93 (s, 2H), 7.69 (d, *J* = 7.9 Hz, 2H), 7.35 (t, *J* = 7.7 Hz, 2H), 7.29 (q, *J* = 9.5, 9.1 Hz, 14H), 7.20 (dd, *J* = 14.2, 8.0 Hz, 16H), 7.16-7.09 (m, 4H), 7.08-6.97 (m, 10H), 6.87 (d, *J* = 1.9 Hz, 2H), 6.74 (d, *J* = 1.9 Hz, 2H). ^{13}C NMR data for *g*-DABNA-Cz-Br could not be obtained due to its poor solubility in all conventional deuterated solvents. MALDI-TOF MS: m/z: 1234.70 [M]+ (calcd: 1234.28). Anal. Calcd for $C_{78}H_{54}Br_2N_6$: C, 75.85; H, 4.41; Br, 12.94; N, 6.80. Found: C, 75.82; H, 4.40; N, 6.83.

Synthesis of *g*-DABNA-Cz: *g*-DABNA-Cz was synthesized by replacing *g*-DABNA-Br with *g*-DABNA-Cz-Br according to the synthetic procedure of *g*-DABNA. The crude product was purified by column chromatography with dichloromethane/petroleum (1: 2) as eluent to afford *g*-DABNA-Cz as an orange solid (yield = 1.1 g, 36%). ^{1}H NMR (600 MHz, CD_2Cl_2) δ 10.67 (s, 2H), 9.53 (d, *J* = 7.7 Hz, 2H), 9.13 (d, *J* = 8.4 Hz, 2H), 7.70 (ddd, *J* = 31.5, 15.4, 7.8 Hz, 6H), 7.58 (dd, *J* = 18.2, 7.4 Hz, 8H), 7.36 (d, *J* = 7.4 Hz, 4H), 7.27 (dt, *J* = 22.6, 7.5 Hz, 10H), 7.16 (d, *J* = 7.9 Hz, 10H), 7.06 (t, *J* = 7.4 Hz, 4H), 6.31 (s, 2H). ^{13}C NMR data for *g*-DABNA-Cz could not be obtained due to its poor solubility in all conventional deuterated solvents. HRMS (MALDI-FTICR): m/z: 1092.4274 [M]+ (calcd:1092.4300). Anal. Calcd for $C_{78}H_{50}B_2N_6$: C, 85.72; H, 4.61; B, 1.98; N, 7.69. Found: C, 85.73; H, 4.61; N, 7.66.

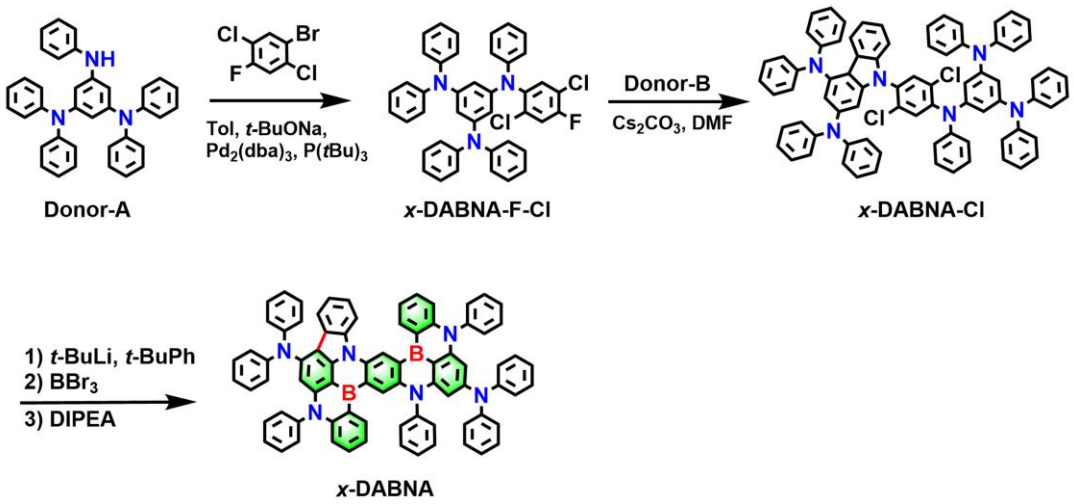

Scheme S5. Synthetic procedures of *x*-DABNA.

Synthesis of *x*-DABNA-F-Cl: Donor-A (11.1 g, 22.0 mmol), *t*-BuONa (3.5 g, 36.0 mmol), 1-bromo-2,5-dichloro-4-fluorobenzene (4.9 g, 20.0 mmol), $Pd_2(dba)_3$ (0.5 g, 0.5 mmol) and $P(tBu)_3$ (0.2 g, 1 mmol) were dissolved in Tol (50 mL). The mixture was stirred at 110 ºC for 12 h under nitrogen. After cooling to room temperature, the resulting product was diluted with chloroform and washed with water. The combined organic extracts were dried over Na_2SO_4 and concentrated under reduced pressure. The crude product was purified by column chromatography with dichloromethane/petroleum (1: 5) as eluent to afford *x*-DABNA-F-Cl as a white solid (yield = 12.1 g, 91%). ^{1}H NMR (600 MHz, CD_2Cl_2) δ 7.24 (dd, *J* = 7.4, 1.2 Hz, 1H), 7.21-7.13 (m, 11H), 7.04-7.00 (m, 8H), 6.93 (t, *J* = 7.2 Hz, 4H), 6.90 (t, *J* = 7.8 Hz, 3H), 6.35 (s, 1H), 6.20 (s, 2H). ^{13}C NMR (151 MHz, $CDCl_3$) δ 156.28, 154.61, 149.13, 147.63, 147.18, 145.91, 140.61, 131.70, 129.09, 129.05, 124.03, 122.76, 122.60, 121.85, 120.30, 120.18, 118.99, 118.82, 113.85, 111.96. MALDI-TOF MS: m/z: 665.35 [M]+ (calcd: 665.18). Anal. Calcd for $C_{42}H_{30}Cl_2FN_3$: C, 75.67; H, 4.54; Cl, 10.64; F, 2.85; N, 6.30. Found: C, 75.68; H, 4.54; N, 6.28.

Synthesis of *x*-DABNA-Cl: *x*-DABNA-F-Cl (6.7 g, 10.0 mmol), Cs_2CO_3 (6.5 g, 20.0 mmol) and Donor-B (5.5 g, 11.0 mmol) were dissolved in DMF (100 mL). The mixture was stirred at 150 ºC for 12 h under nitrogen. After cooling to room temperature, the resulting product was diluted with chloroform and washed with water. The combined organic extracts were dried over Na_2SO_4 and concentrated under reduced pressure. The crude product was purified by column chromatography with dichloromethane/petroleum (1: 3) as eluent to afford *x*-DABNA-Cl as a

white solid (yield = 9.9 g, 86%). ^{1}H NMR (600 MHz, CD_2Cl_2) δ 7.44 (s, 1H), 7.28 (t, *J* = 7.7 Hz, 1H), 7.23-7.19 (m, 8H), 7.17 (dd, *J* = 10.5, 7.6 Hz, 10H), 7.13 (d, *J* = 8.0 Hz, 4H), 7.05 (dd, *J* = 10.3, 7.9 Hz, 12H), 7.01-6.96 (m, 4H), 6.94 (t, *J* = 7.4 Hz, 8H), 6.75 (d, *J* = 1.8 Hz, 1H), 6.64 (d, *J* = 1.8 Hz, 1H), 6.27 (s, 2H). ^{13}C NMR (151 MHz, $CDCl_3$) δ 149.28, 147.75, 147.55, 147.35, 147.20, 147.12, 145.87, 145.13, 143.31, 141.91, 141.03, 132.76, 132.49, 131.83, 131.10, 130.53, 129.26, 129.20, 129.13, 125.08, 124.17, 123.83, 123.34, 122.96, 122.91, 122.74, 122.45, 122.01, 121.95, 120.62, 118.93, 116.36, 113.96, 112.32, 109.37, 103.17. MALDI-TOF MS: m/z: 1146.50 [M]+ (calcd: 1146.39). Anal. Calcd for $C_{78}H_{56}Cl_2N_6$: C, 81.59; H, 4.92; Cl, 6.17; N, 7.32. Found: C, 51.56; H, 4.88; N, 7.30.

Synthesis of *x*-DABNA: *x*-DABNA was synthesized by replacing *g*-DABNA-Br with *x*-DABNA-Cl according to the synthetic procedure of *g*-DABNA. The crude product was purified by column chromatography with dichloromethane/petroleum (1: 2) as eluent to afford *x*-DABNA as an orange solid (yield = 0.9 g, 28%). ^{1}H NMR (600 MHz, CD_2Cl_2) δ 10.26 (s, 1H), 9.15 (d, *J* = 7.7 Hz, 1H), 8.86 (d, *J* = 8.5 Hz, 1H), 8.50 (s, 1H), 8.08 (d, *J* = 7.9 Hz, 1H), 7.65 (t, *J* = 7.9 Hz, 2H), 7.55 (d, *J* = 7.1 Hz, 2H), 7.52 (d, *J* = 7.8 Hz, 1H), 7.45 (q, *J* = 9.1, 8.1 Hz, 6H), 7.41 (d, *J* = 7.8 Hz, 2H), 7.36 (t, *J* = 8.0 Hz, 2H), 7.30 (d, *J* = 7.3 Hz, 1H), 7.22 (d, *J* = 7.7 Hz, 2H), 7.15 (d, *J* = 7.5 Hz, 2H), 7.09 (dd, *J* = 14.0, 7.5 Hz, 10H), 6.99 (d, *J* = 8.2 Hz, 5H), 6.95-6.87 (m, 10H), 6.75 (d, *J* = 8.7 Hz, 1H), 6.10 (s, 1H). ^{13}C NMR data for *x*-DABNA could not be obtained due to its poor solubility in all conventional deuterated solvents. HRMS (MALDI-FTICR): m/z: 1094.4423 [M]+ (calcd:1094.4457). Anal. Calcd for $C_{78}H_{52}B_2N_6$: C, 85.56; H, 4.79; B, 1.97; N, 7.68. Found: C, 85.53; H, 4.81; N, 7.68.

4. Device Fabrication and Measurements

The indium tin oxide (ITO) glass substrates with a sheet resistance of 15 Ω per square were cleaned with optical detergent, deionized water, acetone and isopropanol successively, and then treated with plasma for 5 minutes. Subsequently, they were transferred to a vacuum chamber. Under high vacuum (< 8×10^{-5} Pa), the organic materials were deposited onto the ITO glass substrates at a rate of 1.0 Å s^{-1}. After finishing the deposition of organic layers, ITO glass substrates were patterned by a shadow mask with an array of 2.0 mm × 2.5 mm openings. Then Liq and Al were successively deposited at a rate of 0.1 and 5.0 Å s^{-1}, respectively. The electroluminescence properties of the mono-boron emitters were evaluated using the following device structure: ITO/TAPC (45 nm)/TCTA (5 nm)/MCP (5 nm)/emission layer (EML, 30 nm)/DPEPO (5 nm)/TmPyPb (30 nm)/LiF (1 nm)/Al (100 nm). Here, TAPC (1,1-bis(4-di-p-tolylaminophenyl)cyclohexane) served as the hole transport layer, TCTA (4,4',4"-tris(carbazol-9-yl)-triphenylamine) and MCP (1,3-di(9*H*-carbazol-9-yl)benzene) as exciton blocking layers, DPEPO (bis[2-(diphenylphosphino)phenyl]ether oxide) as a blocking layer, TmPyPb (1,3,5-tri[(3-pyridyl)-phen-3-yl]benzene) as the electron transport layer, and LiF/Al as the cathode. The emission layer consisted of 1 wt% of the mono-boron emitter doped into PhCzBCz (9-(2-(9-phenyl-9*H*-carbazol-3-yl)phenyl)-9*H*-3,9'-bicarbazole). The EL spectrum, CIE coordinate and luminance intensity of the OLEDs were recorded by Photo Research PR655, meanwhile, the current density (*J*) and driving voltage (*V*) were recorded by Keithley 2400. By assuming Lambertian distribution, the external quantum efficiency (EQE) was estimated according to brightness, electroluminescence spectrum and current density. When assuming the external emission profile is Lambertian distribution, the EQE can be determined by the following equations:

$$\mathrm{EQE} = \frac{N_p}{N_e}$$

$$N_p = \frac{\int L_e(\lambda) \cdot \mathrm{W}(\lambda) \cdot d\lambda}{h \times c} \times \pi \times D$$

$$N_e = \frac{I}{e}$$

Where N_p is the photons number, N_e is the electrons number, $L_e(\lambda)$ is the spectral radiance (W sr^{-1} m^{-2} nm^{-1}), W(λ) is the wavelength, dλ=1, D is the emitting area, *h* is the Planck's constant, *c* is

the speed of light in vacuum, *e* is the elementary charge of electron and *I* is the injected current.

5. Calculation Formulas for the Photophysical Parameters:

The calculation of the kinetic parameters assumes that internal conversion process of the singlet exciton is the main nonradiative decay.[S6-S8]

$$k_r = \Phi_F k_F + \Phi_{TADF} k_{TADF}$$

$$k_{nr} = k_r (1-\Phi_{PL})/\Phi_{PL}$$

$$k_{ISC} = k_F - k_r - k_{nr}$$

$$k_{RISC} = (k_F k_{TADF} \Phi_{TADF})/(k_{ISC} \Phi_F)$$

Where k_F and k_{TADF} represent the decay rate constants for prompt and delayed fluorescence, respectively, which are in reciprocal relationship with the decay time constants (τ_F and τ_{TADF}) experimentally determined from transient PL characteristics; Φ_{PL} is the total fluorescence quantum yield, Φ_F is the prompt fluorescent component of Φ_{PL}, Φ_{TADF} is the delayed fluorescent component of Φ_{PL}. k_r, k_{nr}, k_{ISC} and k_{RISC} are rate constants of radiative decay, non-radiative decay, intersystem crossing and reverse intersystem crossing, respectively.

6. Supplementary Figures

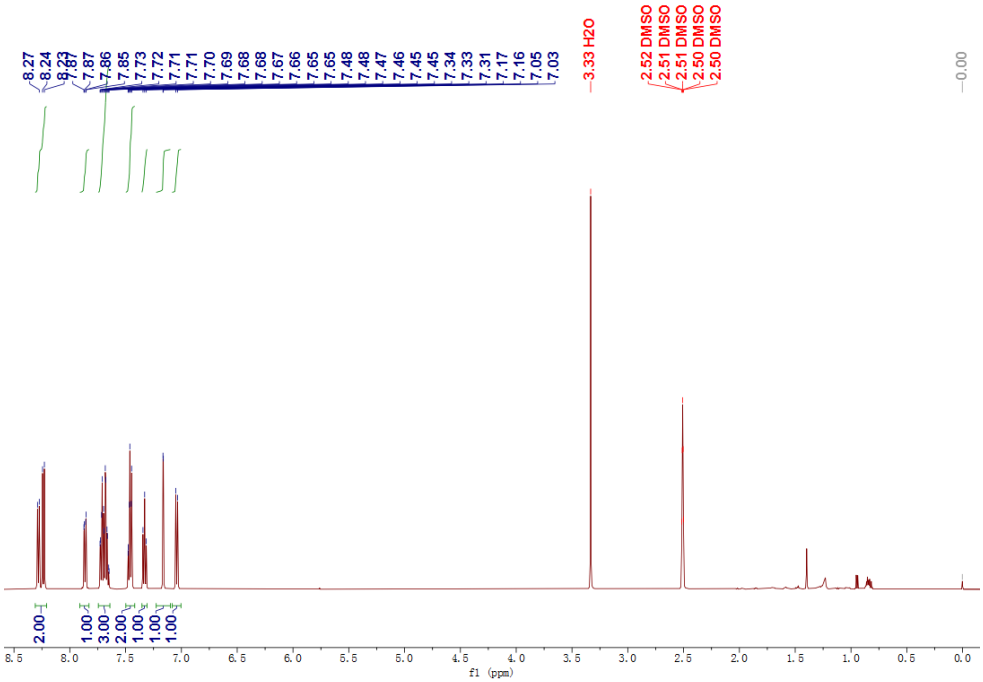

Figure S1. ^{1}H NMR spectrum of Cz-Br (500 MHz, DMSO-d_6).

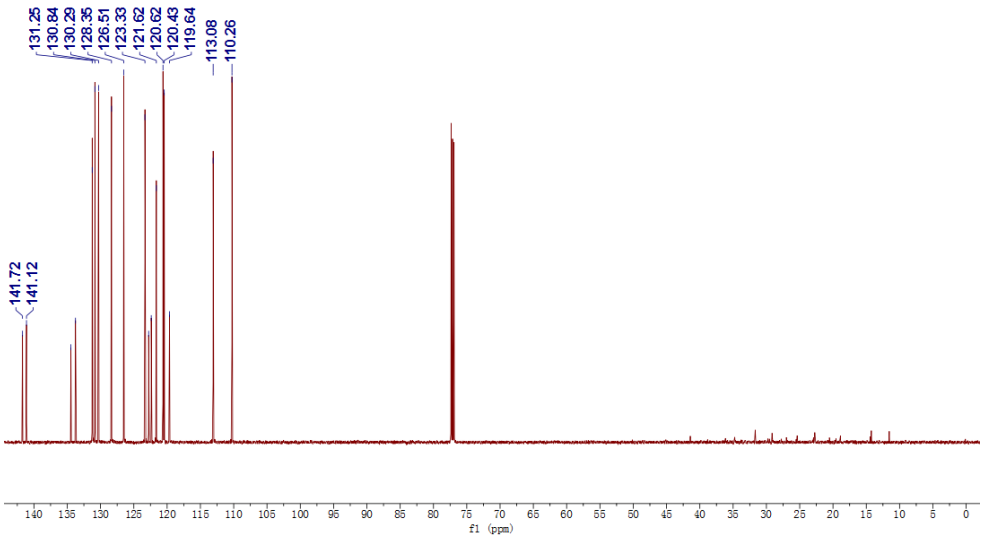

Figure S2. ^{13}C NMR spectrum of Cz-Br (151 MHz, $CDCl_3$).

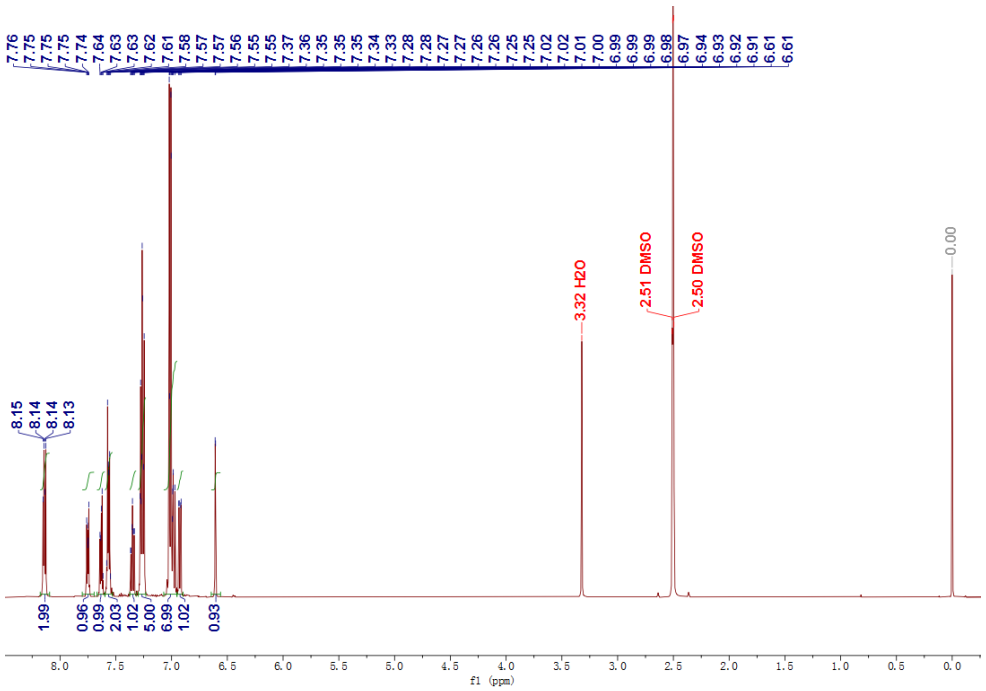

Figure S3. ^{1}H NMR spectrum of Cz-DPA (500 MHz, DMSO-d_6).

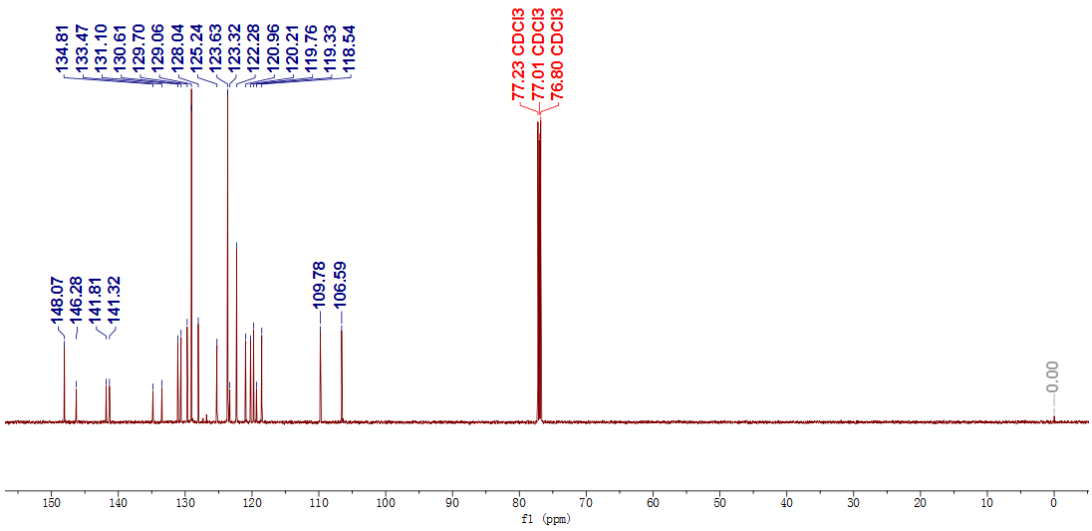

Figure S4. ^{13}C NMR spectrum of Cz-DPA (151 MHz, $CDCl_3$).

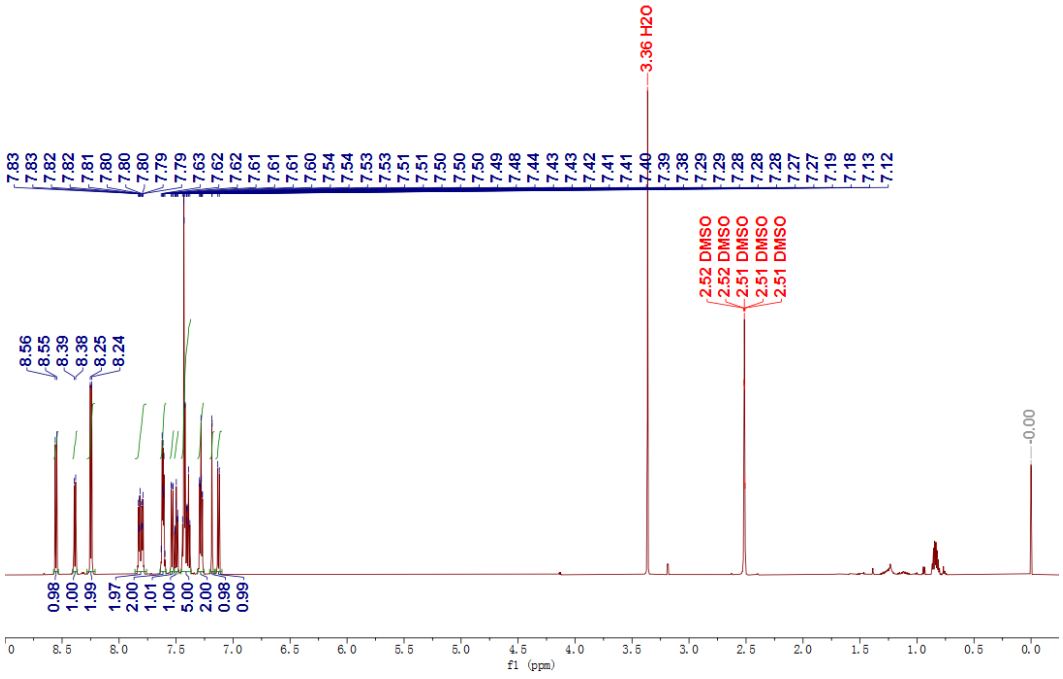

Figure S5. ^{1}H NMR spectrum of Cz-Cz (600 MHz, DMSO-d_6).

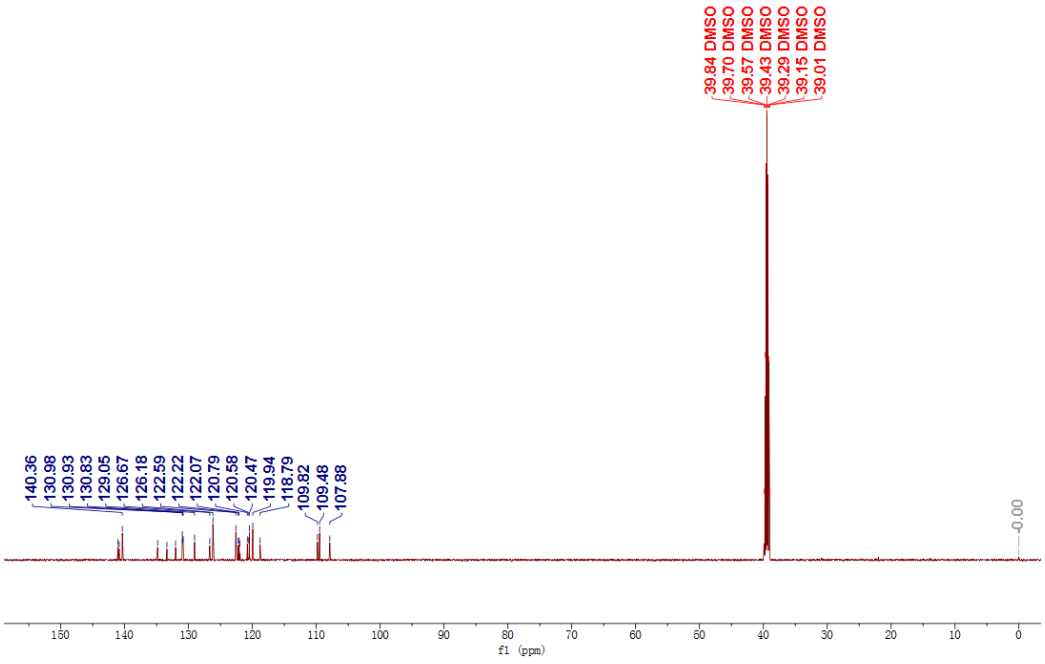

Figure S6. ^{13}C NMR spectrum of Cz-Cz (151 MHz, DMSO-d_6).

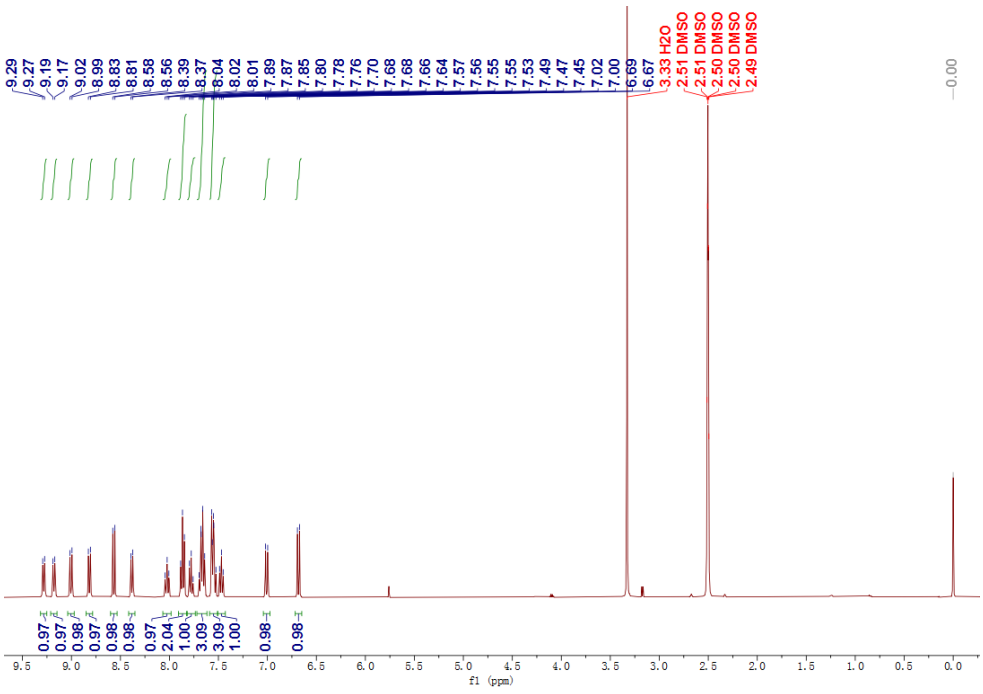

Figure S7. ^{1}H NMR spectrum of MR-Cz-1 (400 MHz, DMSO-d_6).

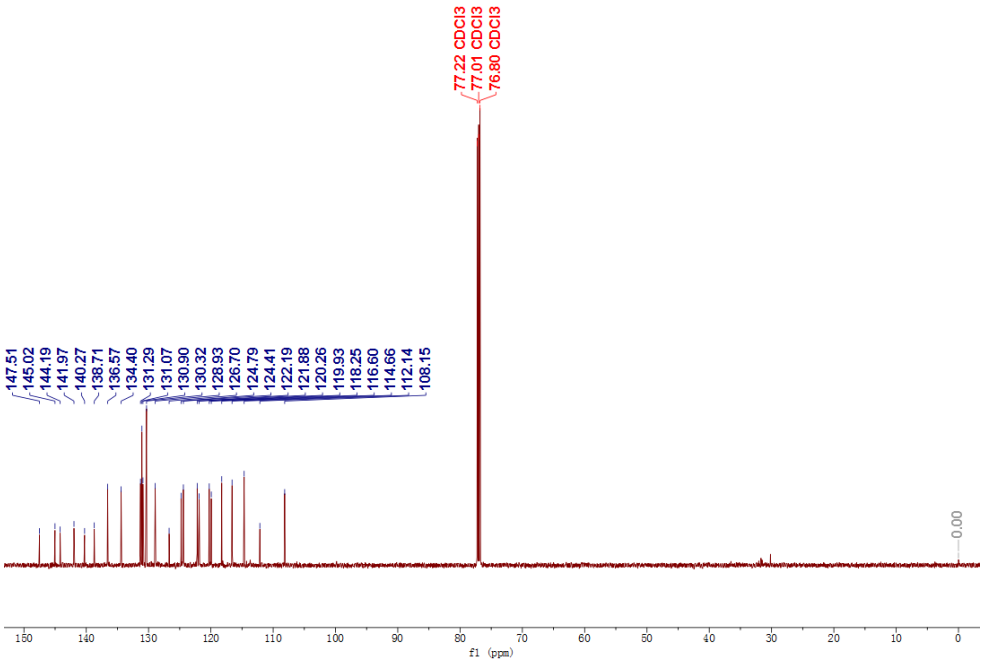

Figure S8. ^{13}C NMR spectrum of MR-Cz-1 (151 MHz, $CDCl_3$).

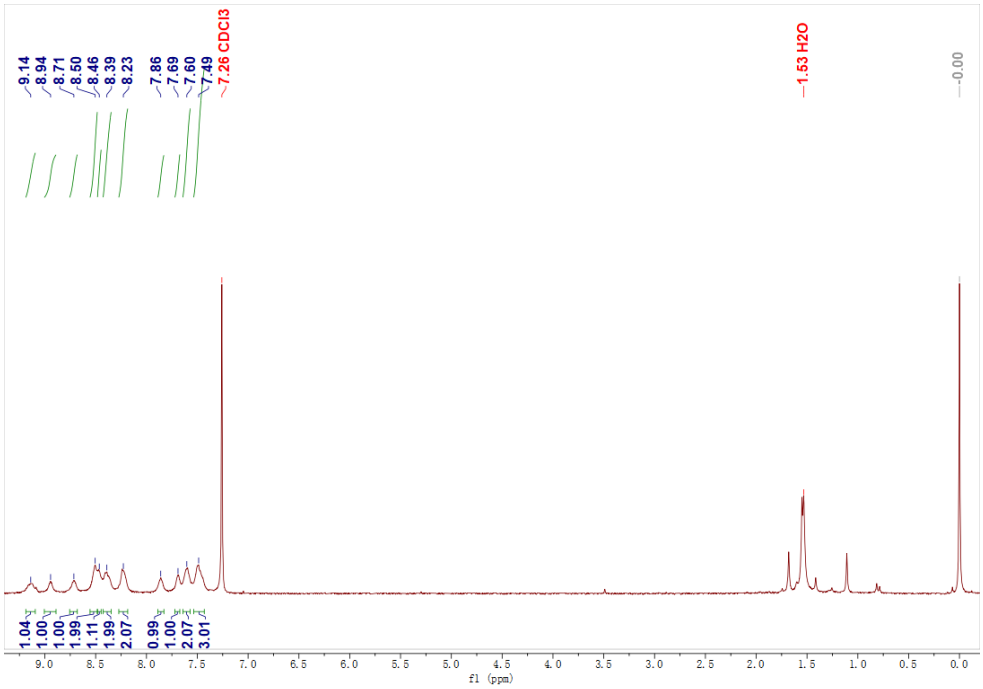

Figure S9. ^{1}H NMR spectrum of MR-DCz-1 (500 MHz, $CDCl_3$).

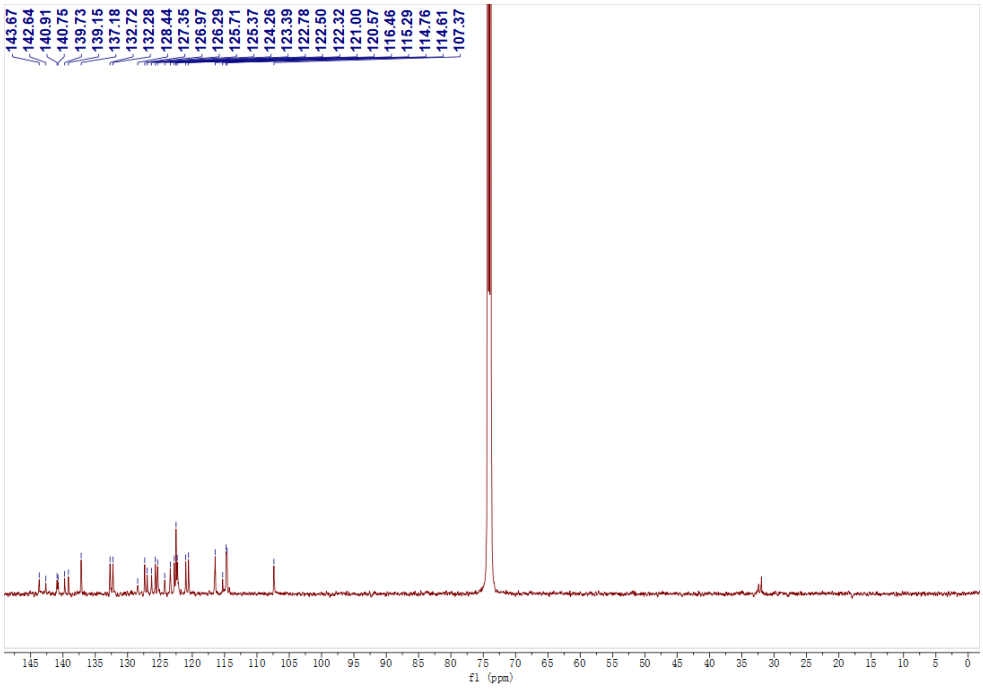

Figure S10. ^{13}C NMR spectrum of MR-DCz-1 (126 MHz, $C_2D_2Cl_4$).

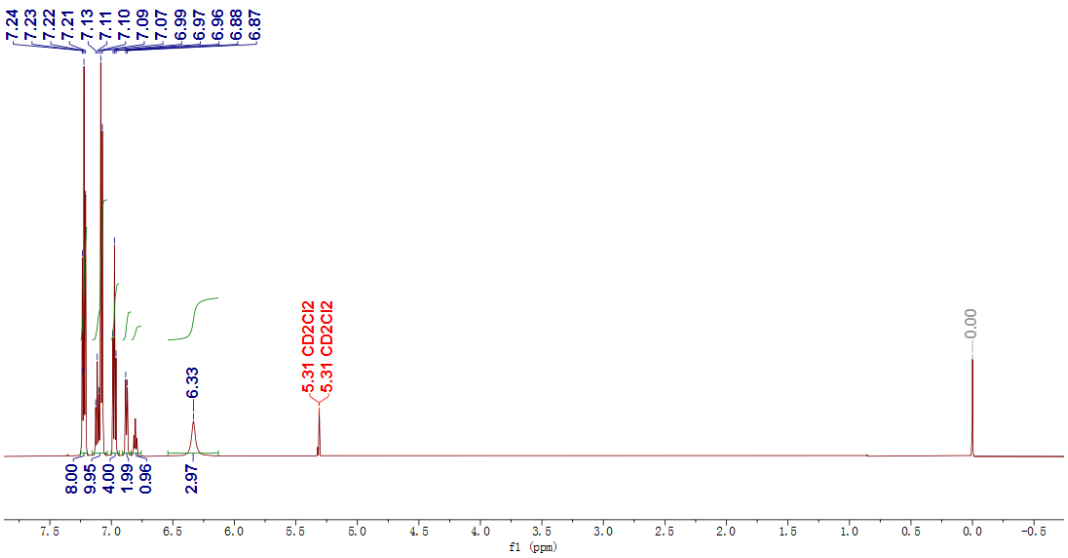

Figure S11. ^{1}H NMR spectrum of Donor-A (600 MHz, CD_2Cl_2).

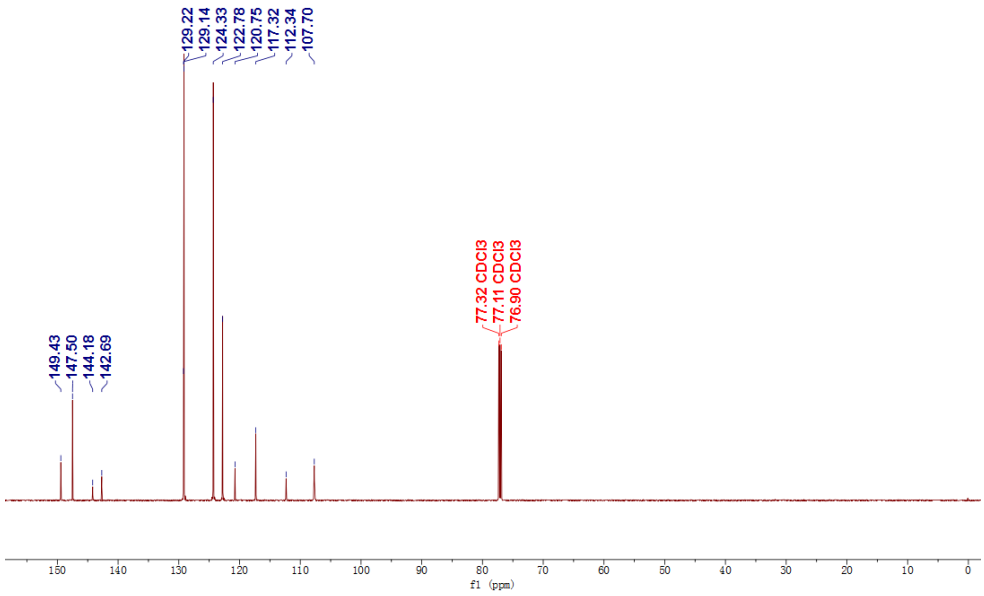

Figure S12. ^{13}C NMR spectrum of Donor-A (151 MHz, $CDCl_3$).

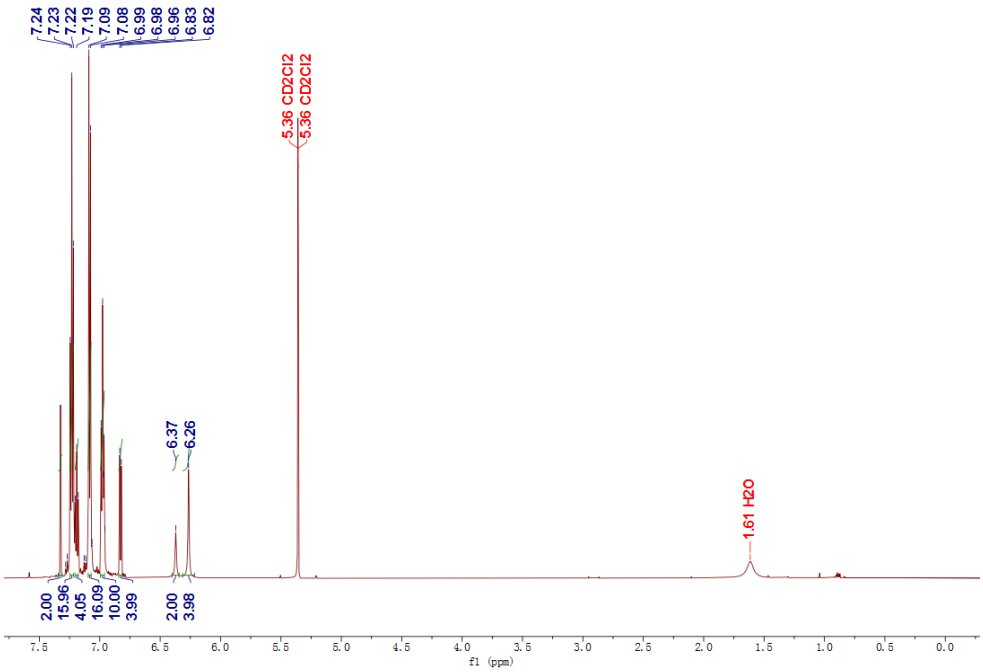

Figure S13. ^{1}H NMR spectrum of *g*-DABNA-Br (600 MHz, CD_2Cl_2).

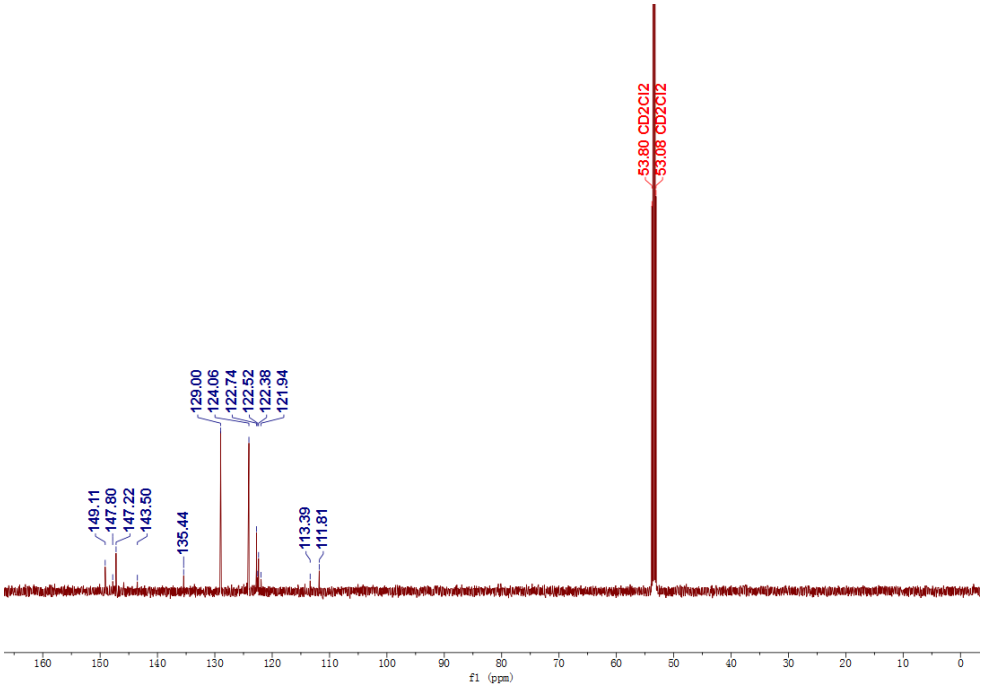

Figure S14. ^{13}C NMR spectrum of *g*-DABNA-Br (151 MHz, CD_2Cl_2).

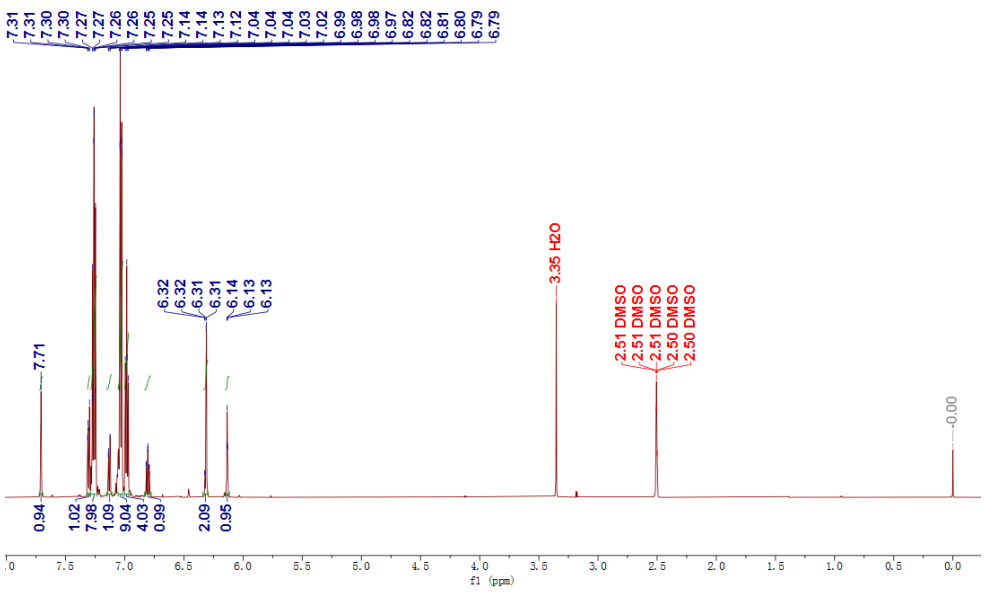

Figure S15. ^{1}H NMR spectrum of Donor-B-Cl (600 MHz, DMSO-d_6).

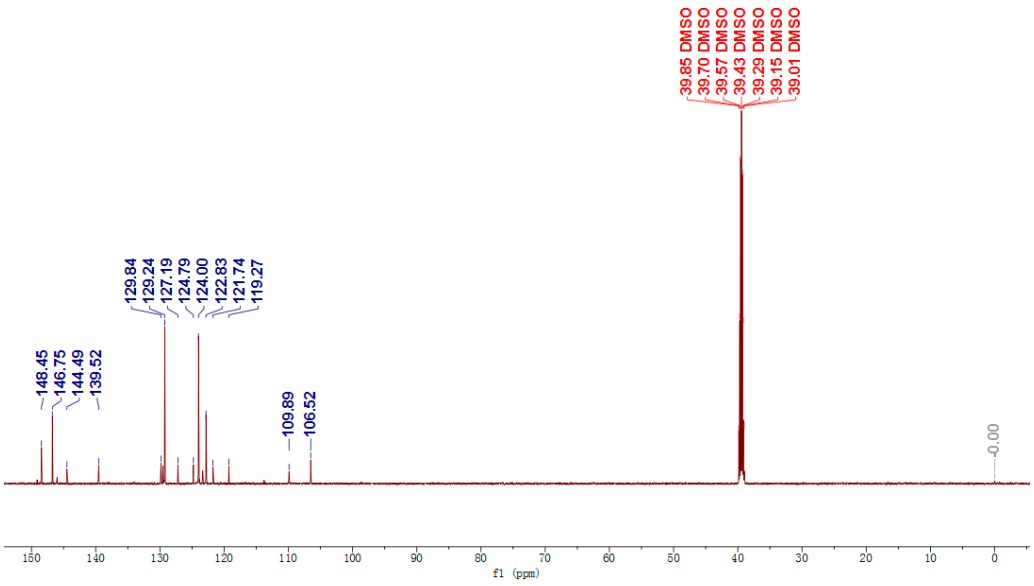

Figure S16. ^{13}C NMR spectrum of Donor-B-Cl (151 MHz, DMSO-d_6).

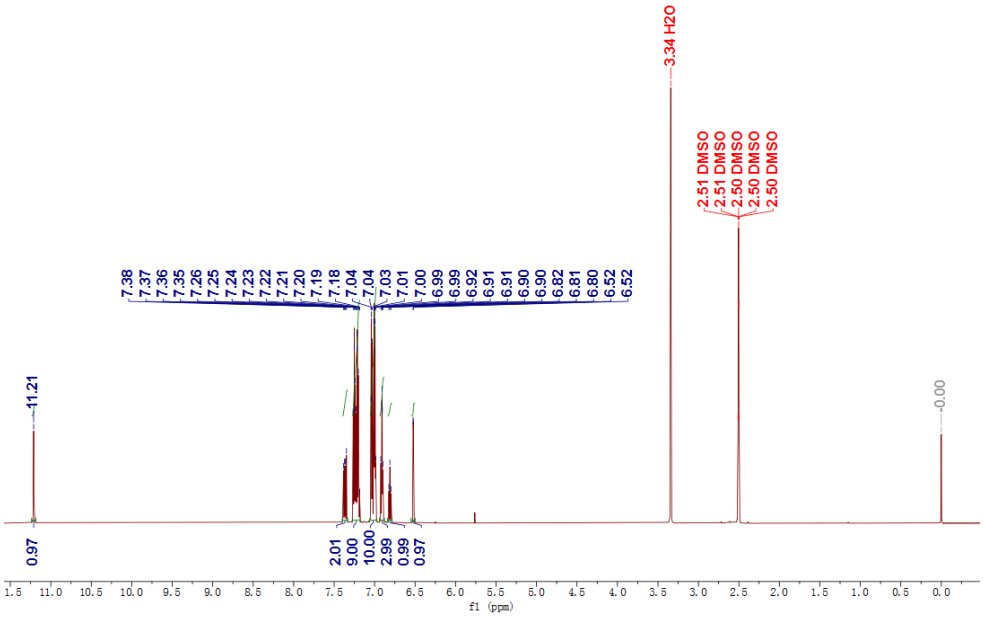

Figure S17. ^{1}H NMR spectrum of Donor-B (600 MHz, DMSO-d_6).

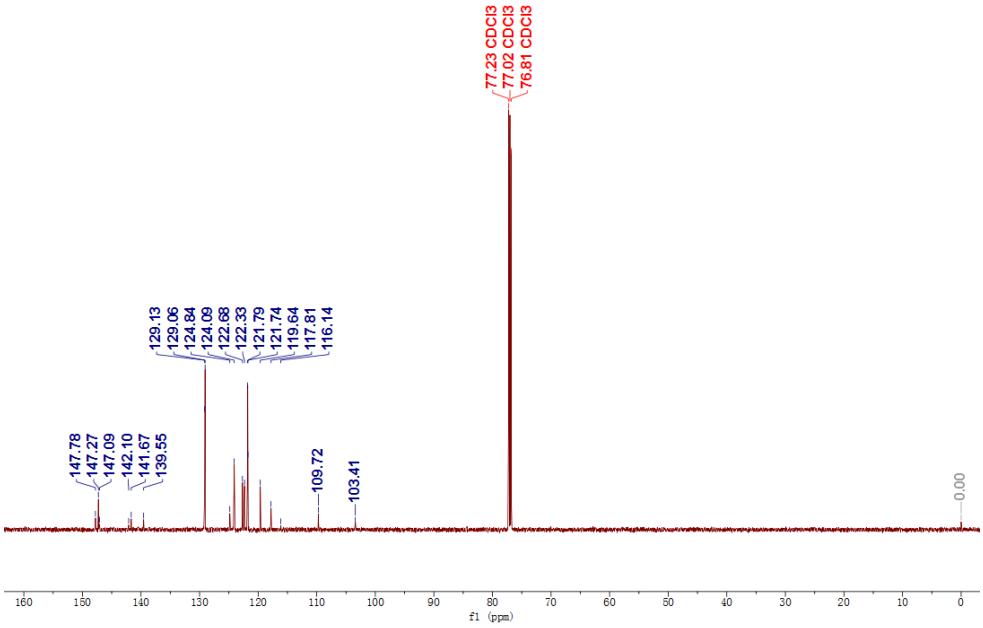

Figure S18. ^{13}C NMR spectrum of Donor-B (151 MHz, $CDCl_3$).

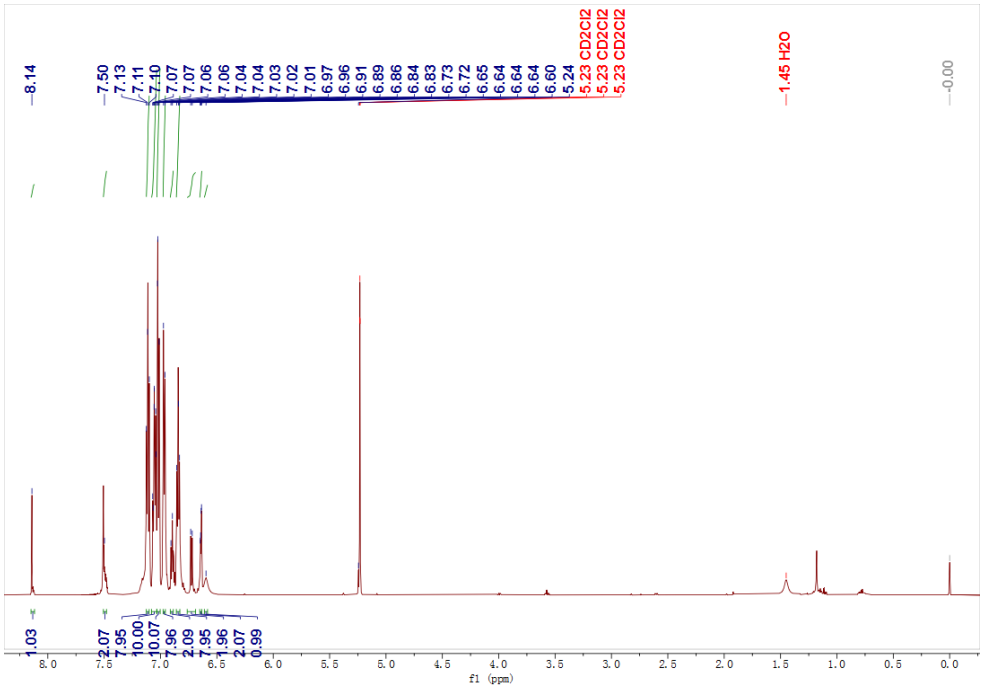

Figure S19. ^{1}H NMR spectrum of *v*-DABNA-Cz-Br (600 MHz, CD_2Cl_2).

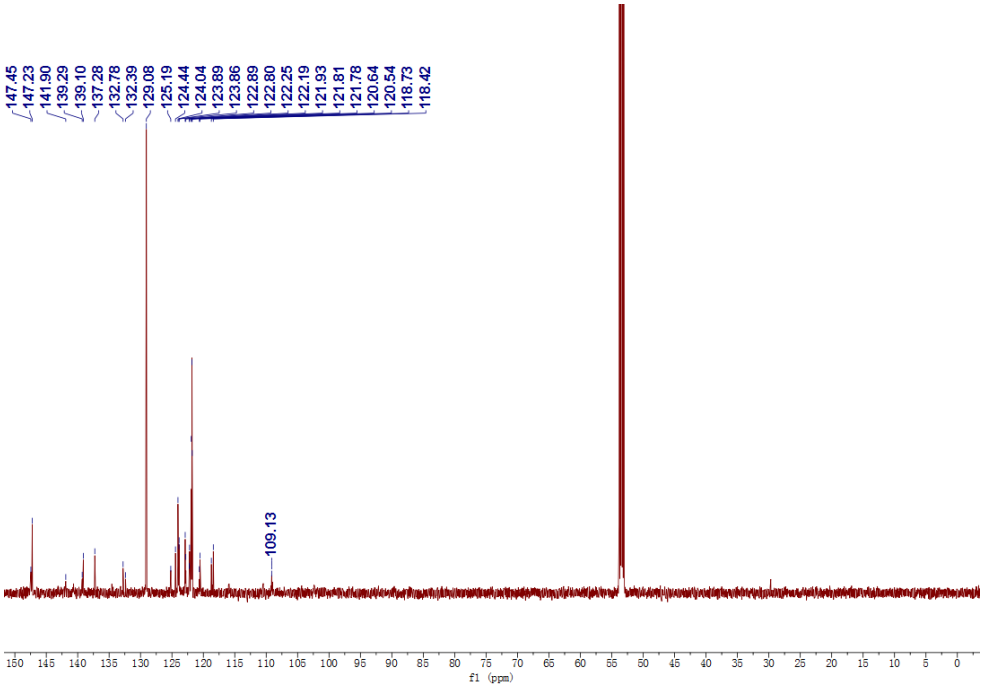

Figure S20. ^{13}C NMR spectrum of *v*-DABNA-Cz-Br (151 MHz, CD_2Cl_2).

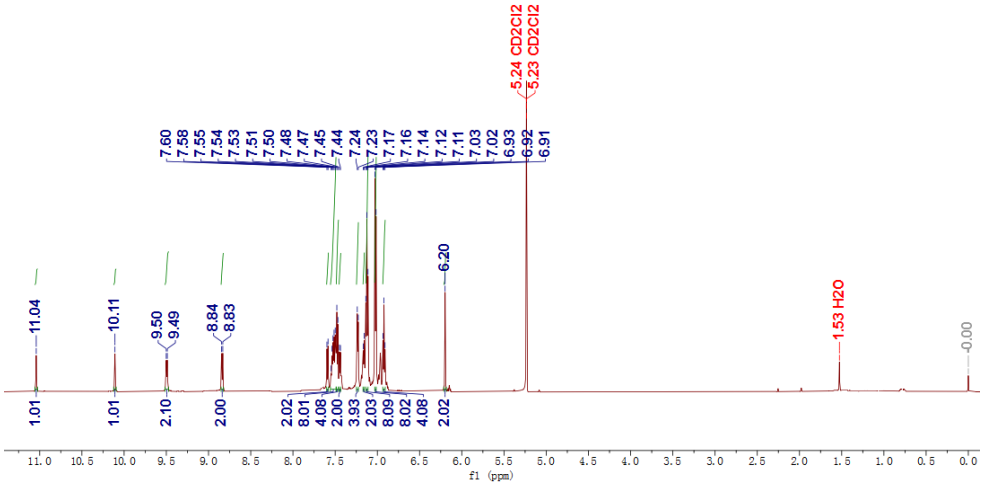

Figure S21. ^{1}H NMR spectrum of *v*-DABNA-Cz (600 MHz, CD_2Cl_2).

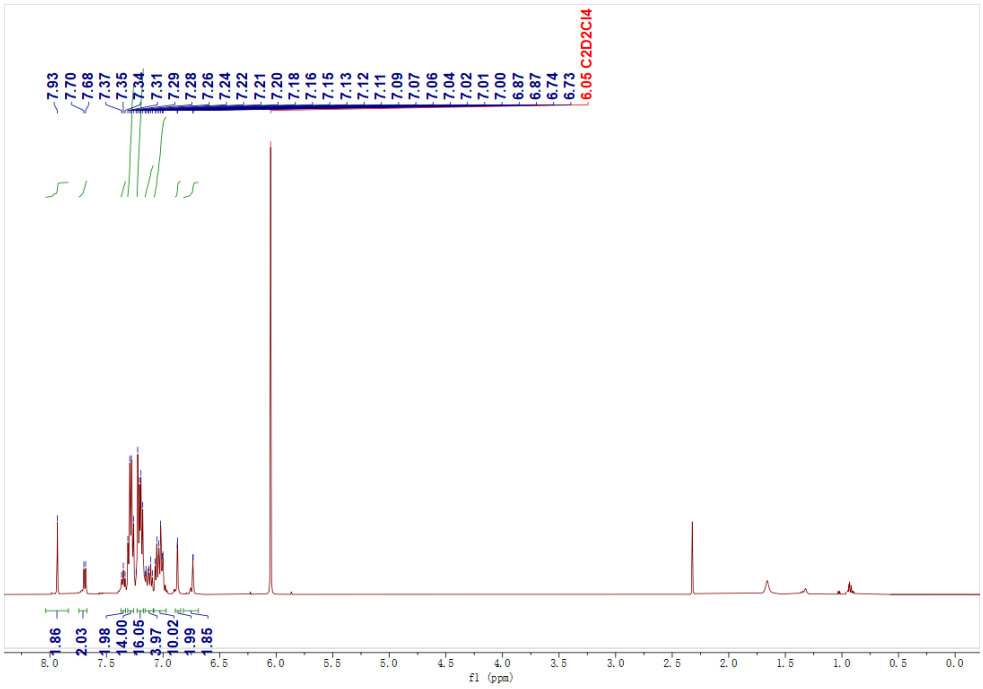

Figure S22. ^{1}H NMR spectrum of *g*-DABNA-Cz-Br (500 MHz, $C_2D_2Cl_4$).

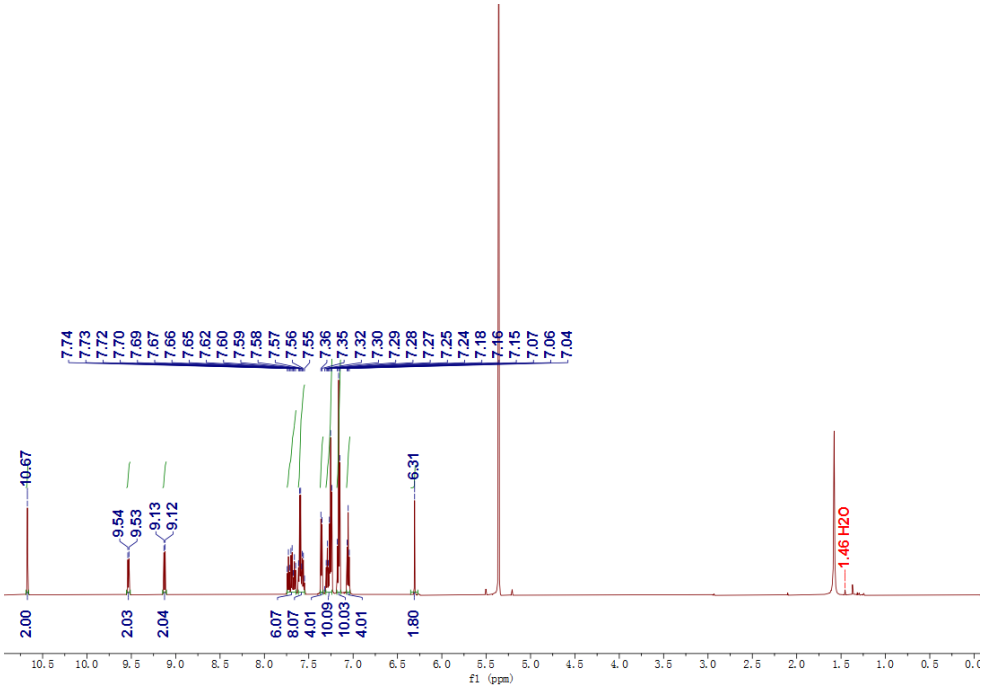

Figure S23. ^{1}H NMR spectrum of *g*-DABNA-Cz (600 MHz, CD_2Cl_2).

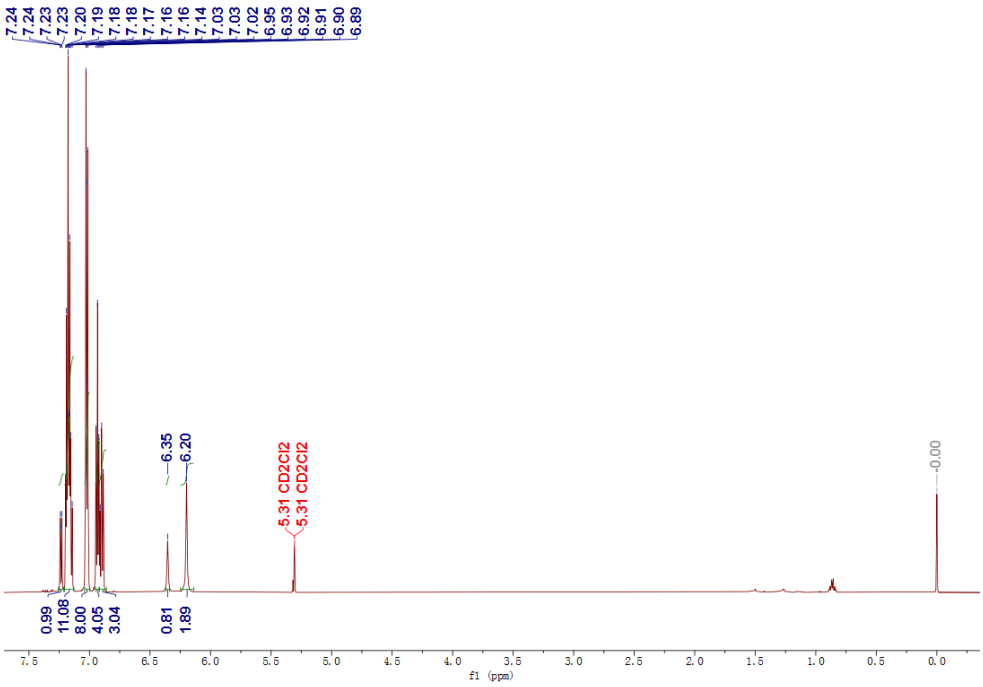

Figure S24. ^{1}H NMR spectrum of *x*-DABNA-F-Cl (600 MHz, CD_2Cl_2).

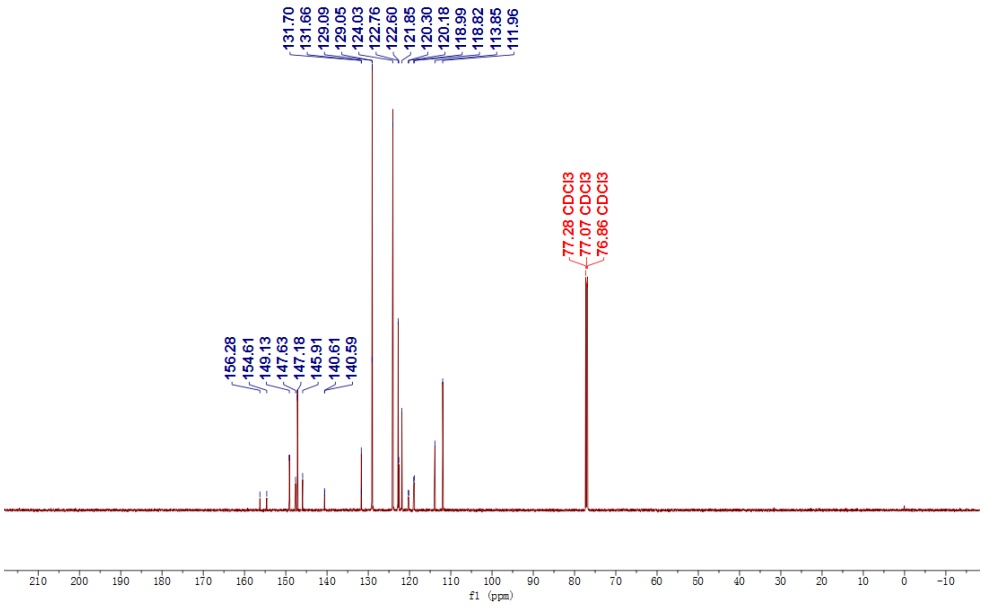

Figure S25. ^{13}C NMR spectrum of *x*-DABNA-F-Cl (151 MHz, $CDCl_3$).

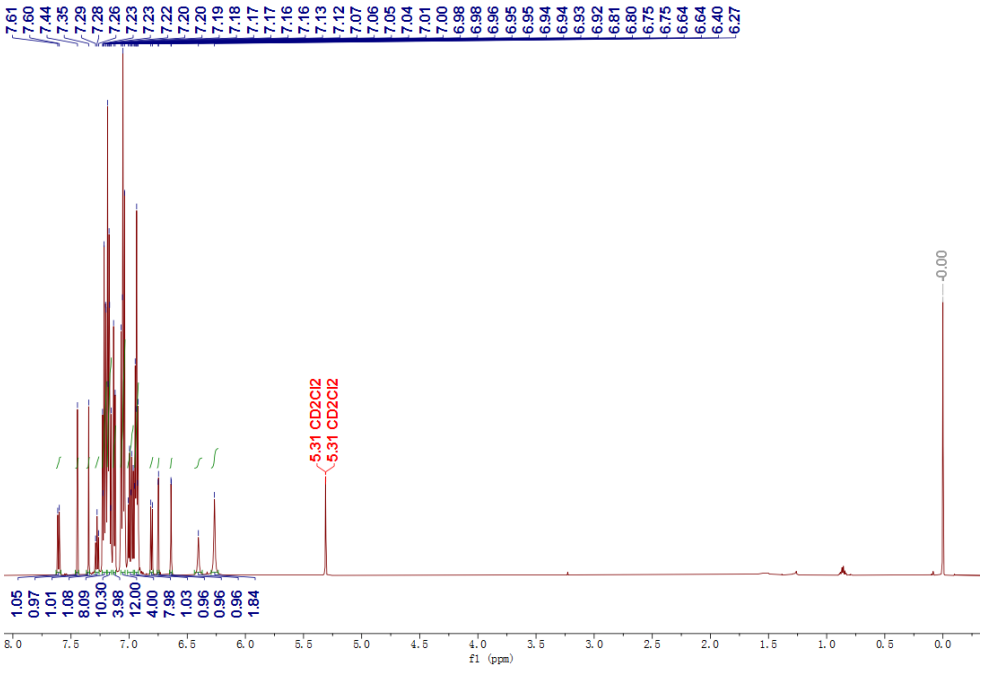

Figure S26. ^{1}H NMR spectrum of *x*-DABNA-Cl (600 MHz, CD_2Cl_2).

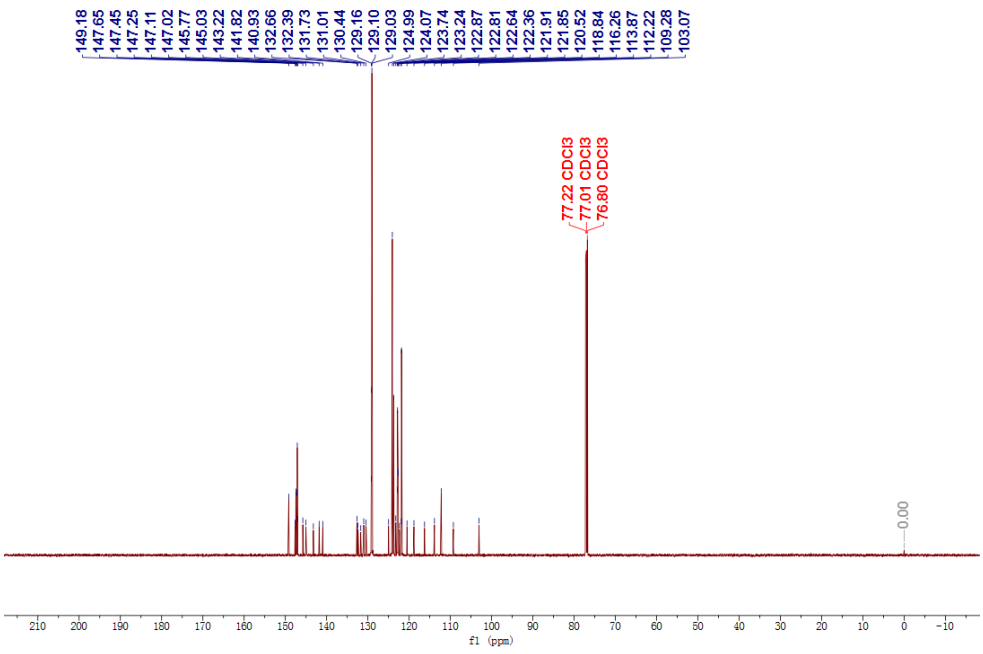

Figure S27. ^{13}C NMR spectrum of *x*-DABNA-Cl (151 MHz, $CDCl_3$).

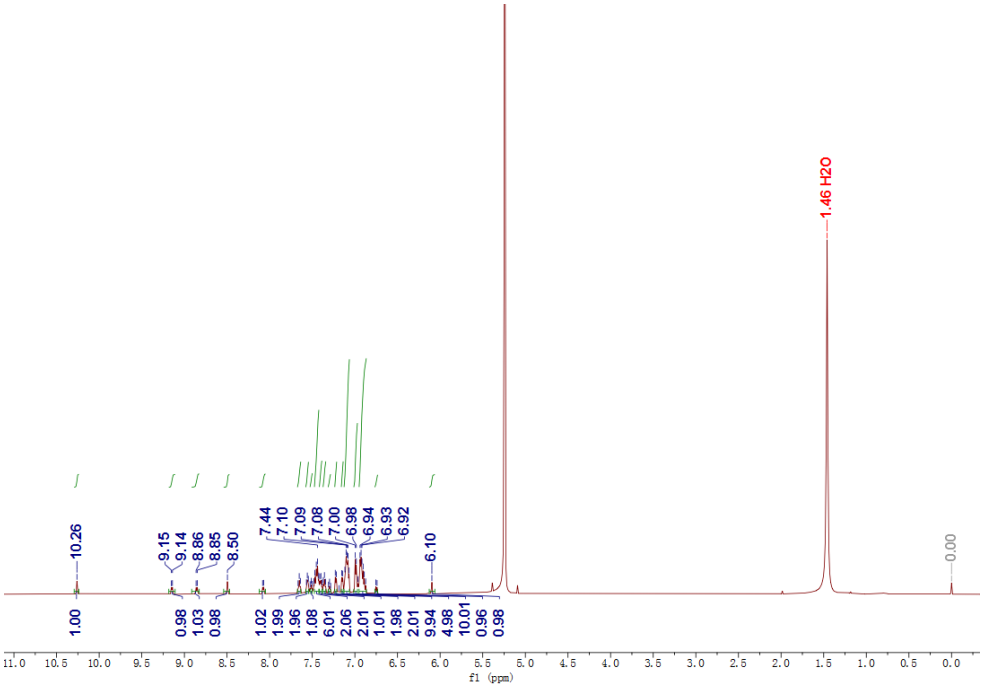

Figure S28. ^{1}H NMR spectrum of *x*-DABNA (600 MHz, CD_2Cl_2).

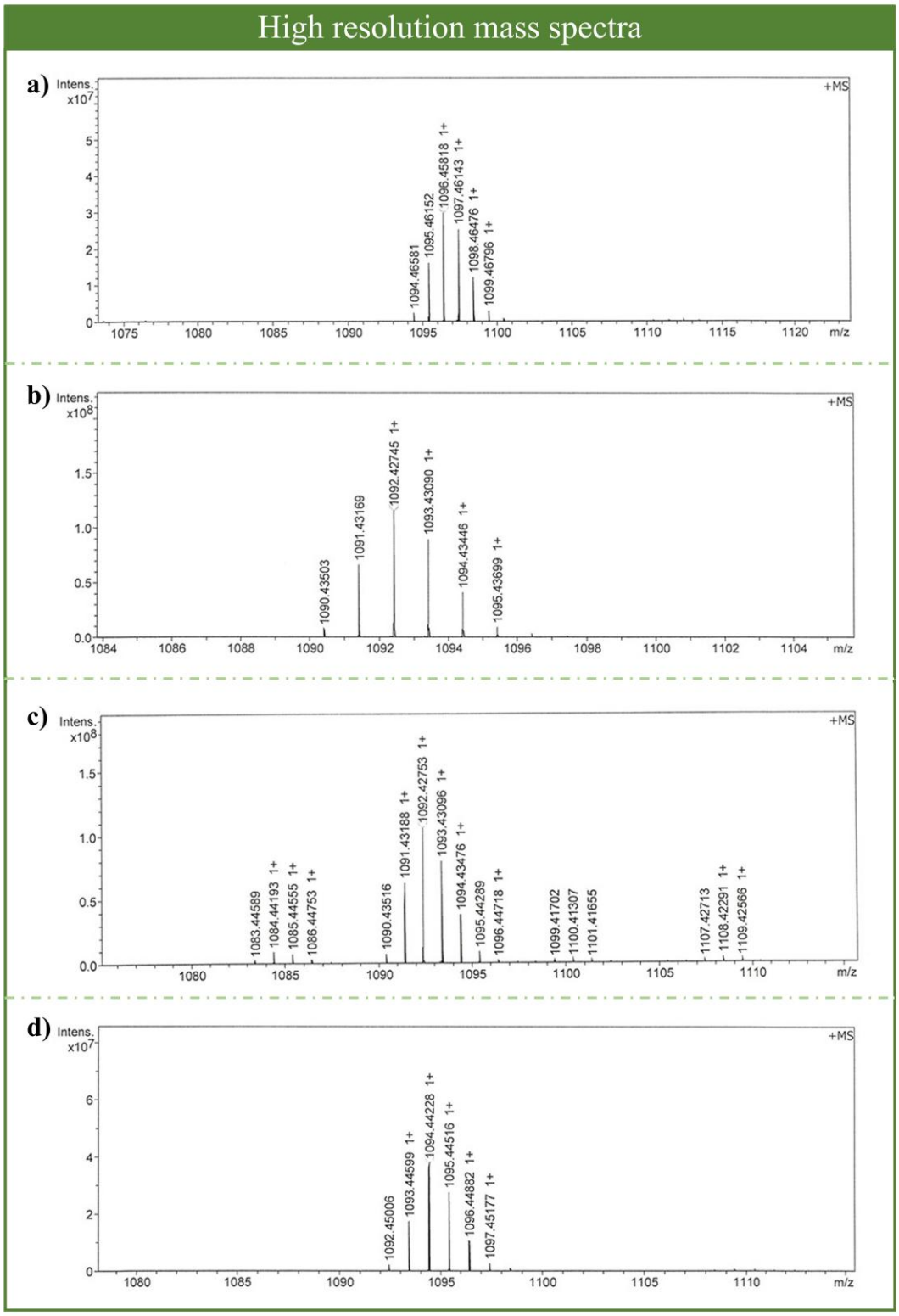

Figure S29. The high resolution mass spectra of a) *g*-DABNA, b) *v*-DABNA-Cz, c) *g*-DABNA-Cz and d) *x*-DABNA.

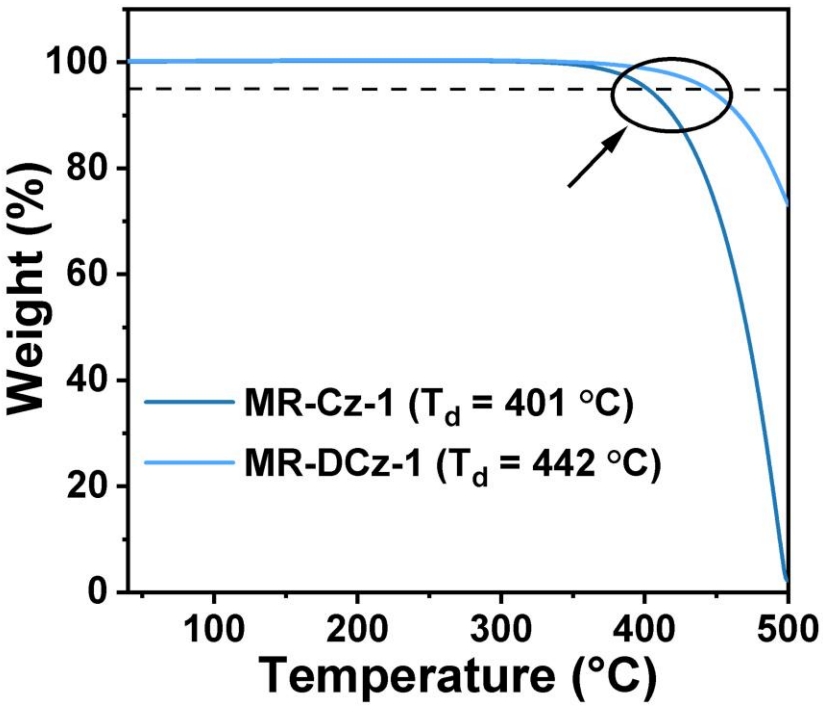

Figure S30. TGA curves of MR-Cz-1 and MR-DCz-1 at a scanning rate of 10 ^{o}C min^{-1} under N_2.

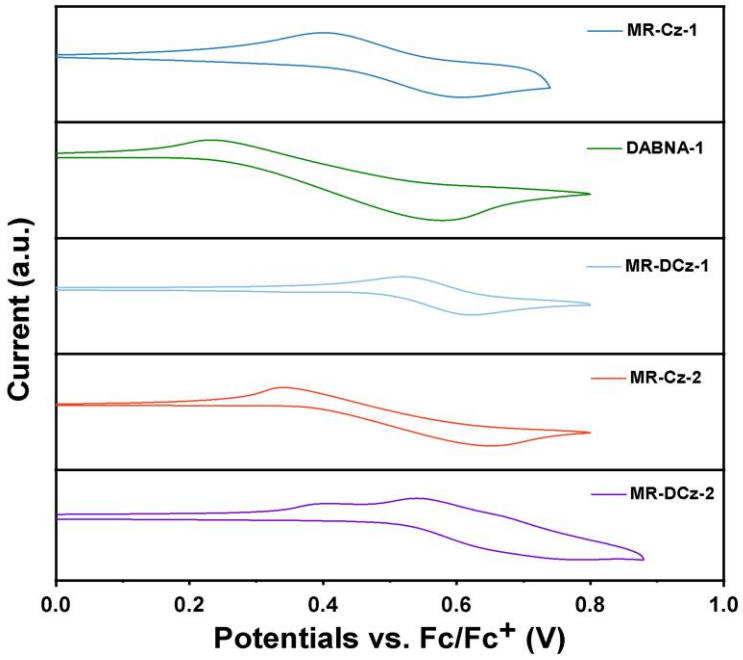

Figure S31. CV curves of MR-Cz-1, DABNA-1, MR-DCz-1, MR-Cz-2 and MR-DCz-2.

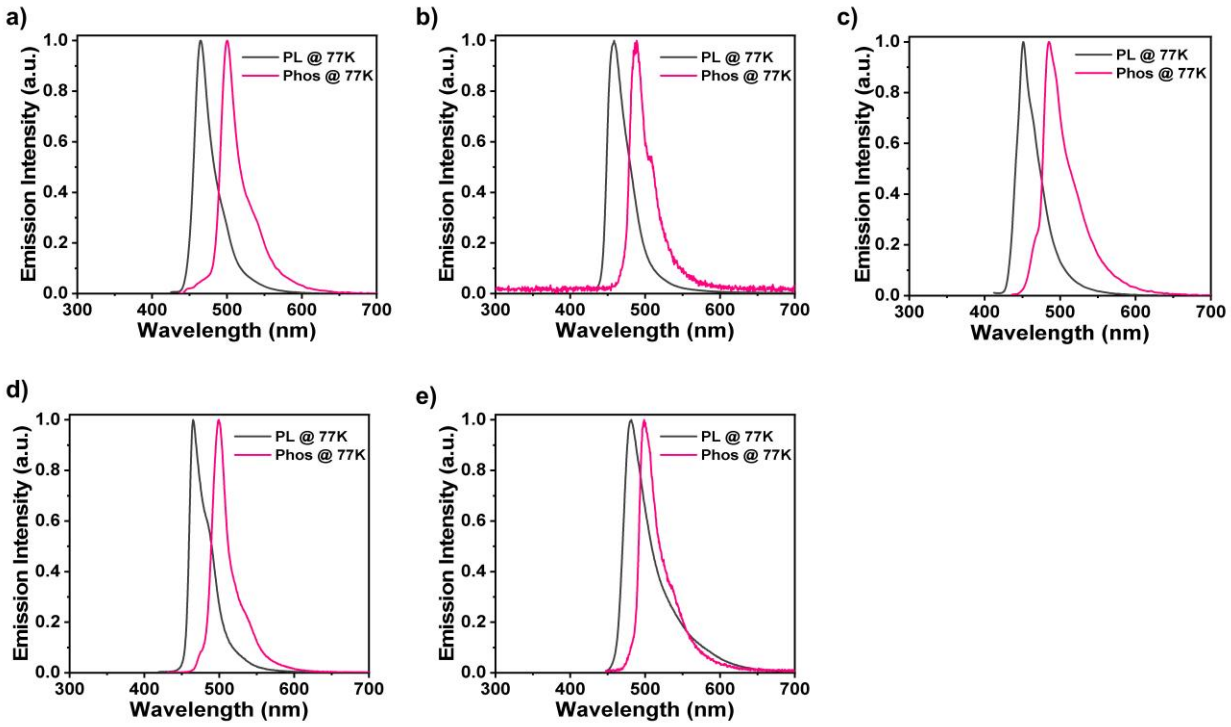

Figure S32. Fluorescence and phosphorescence spectra of a) MR-Cz-1, b) DABNA-1, c) MR-DCz-1, d) MR-Cz-2 and e) MR-DCz-2.

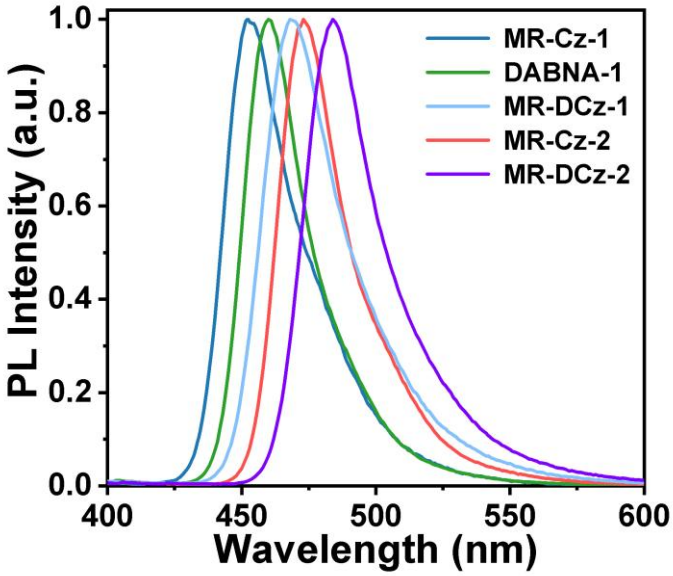

Figure S33. PL spectra of 1 wt% MR-Cz-1, DABNA-1, MR-Cz-2, MR-DCz-1 and MR-DCz-2: PhCzBCz doped films.

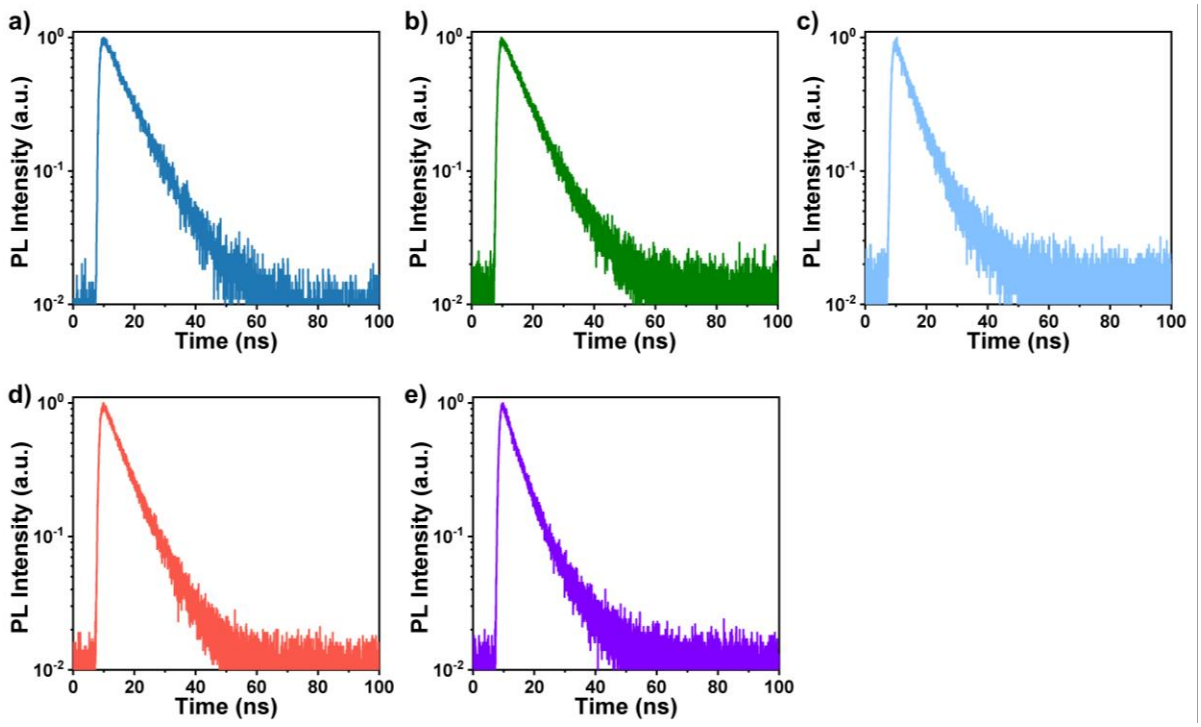

Figure S34. Transient fluorescence decay curves of 1 wt% MR-Cz-1, DABNA-1, MR-Cz-2, MR-DCz-1 and MR-DCz-2: PhCzBCz doped films.

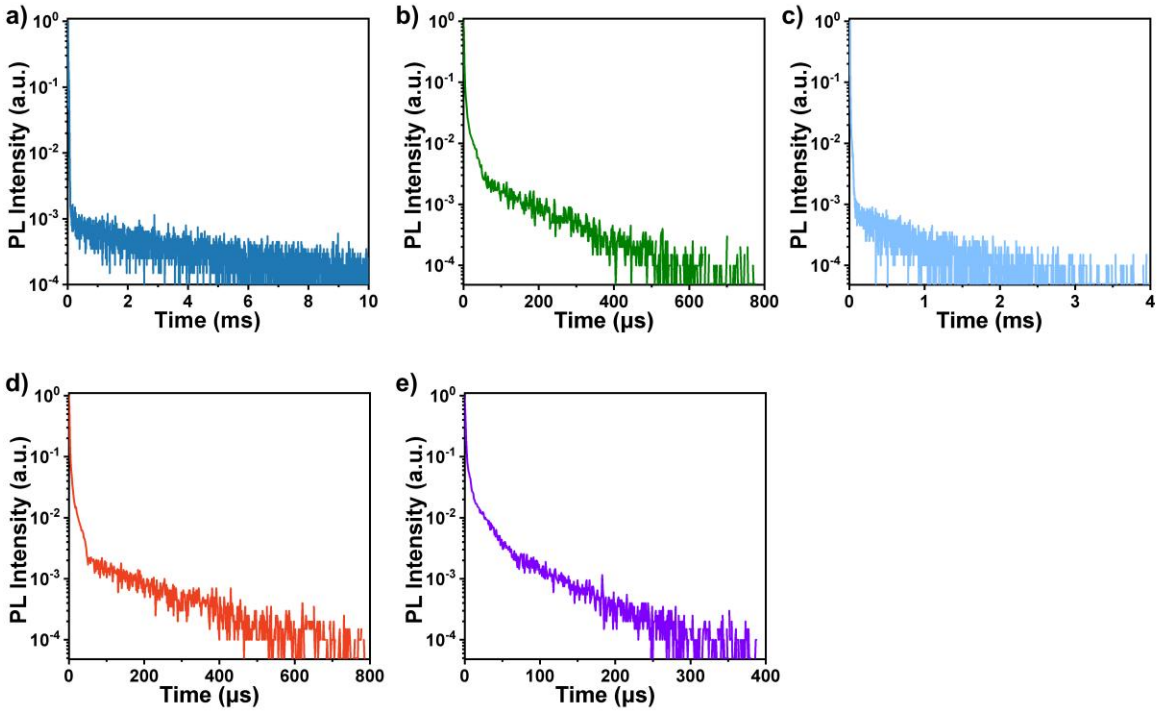

Figure S35. Delayed fluorescence decay curves of 1 wt% MR-Cz-1, DABNA-1, MR-Cz-2, MR-DCz-1 and MR-DCz-2: PhCzBCz doped films.

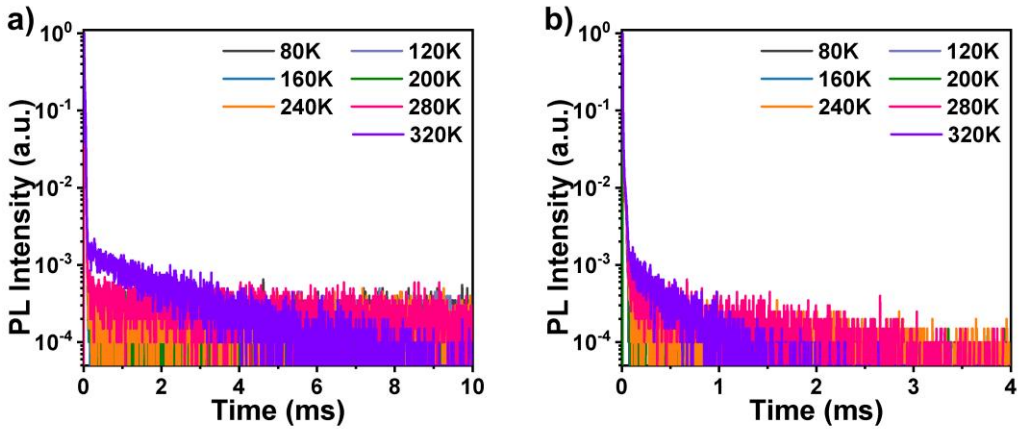

Figure S36. Transition PL decay curves of 1 wt% a) MR-Cz-1 and b) MR-DCz-1: PhCzBCz doped films under different temperatures from 80 to 320 K.

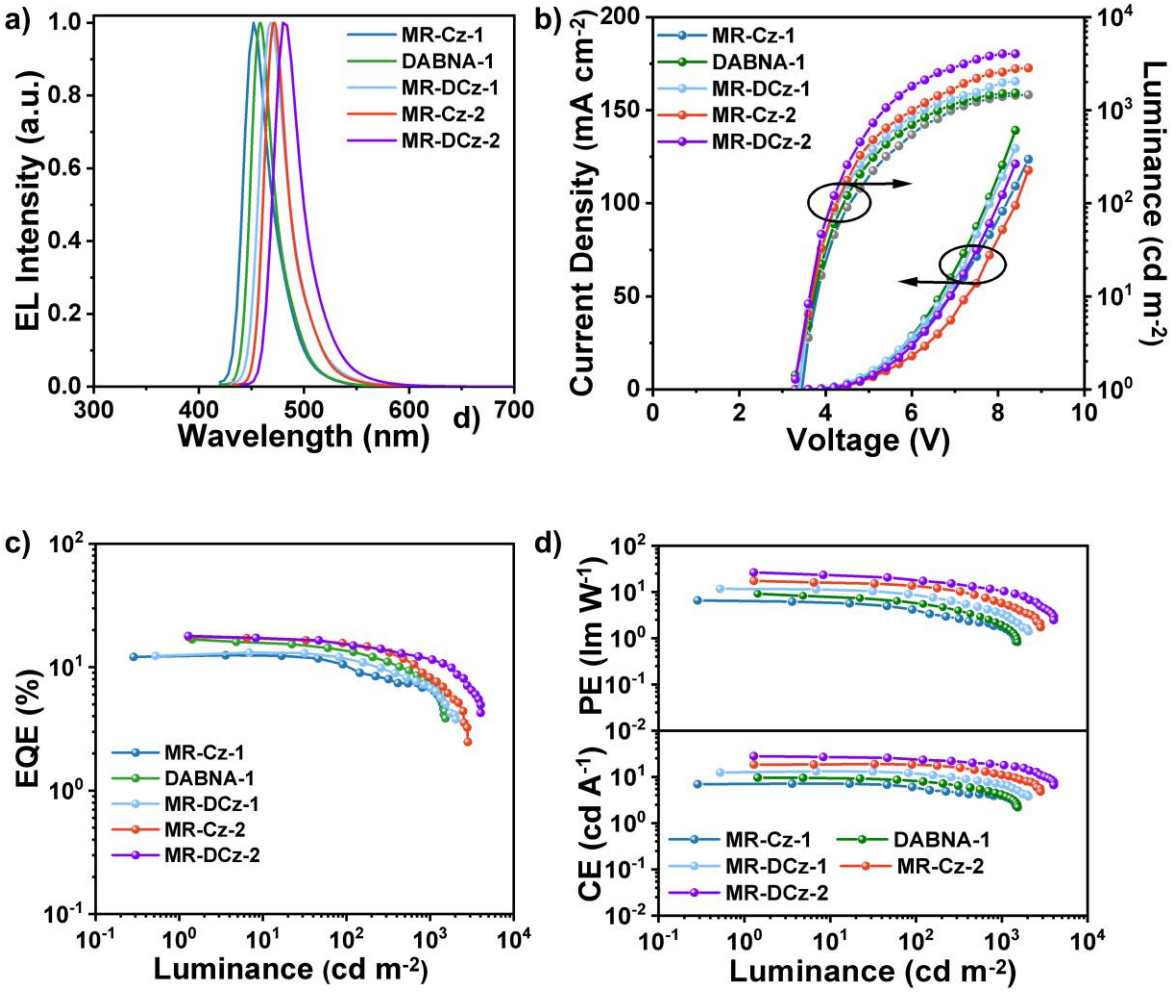

Figure S37. EL characteristics of MR-Cz-1, DABNA-1, MR-Cz-2, MR-DCz-1 and MR-DCz-2. a) EL spectra. b) *J*-*V*-*L* curves. c) EQE-*L* curves. d) CE-*L* and PE-*L* curves.

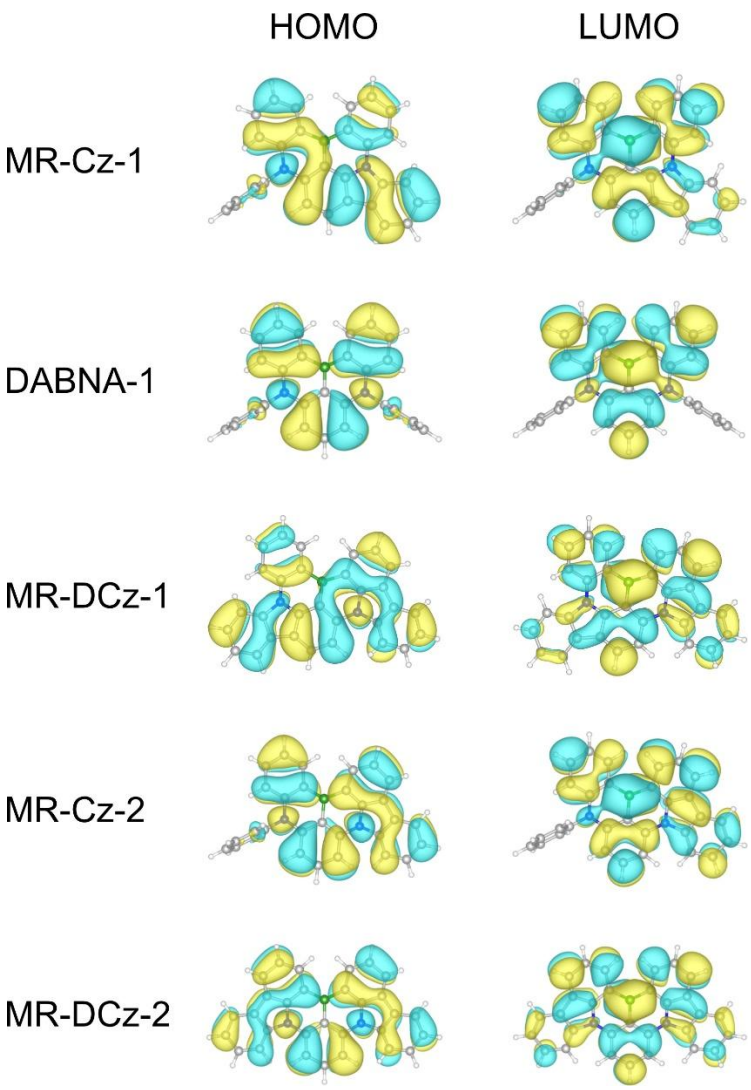

Figure S38. Frontier molecular orbitals of model MR-TADF molecules calculated and visualized at Hartree-Fock/def2-TZVP level of theory.

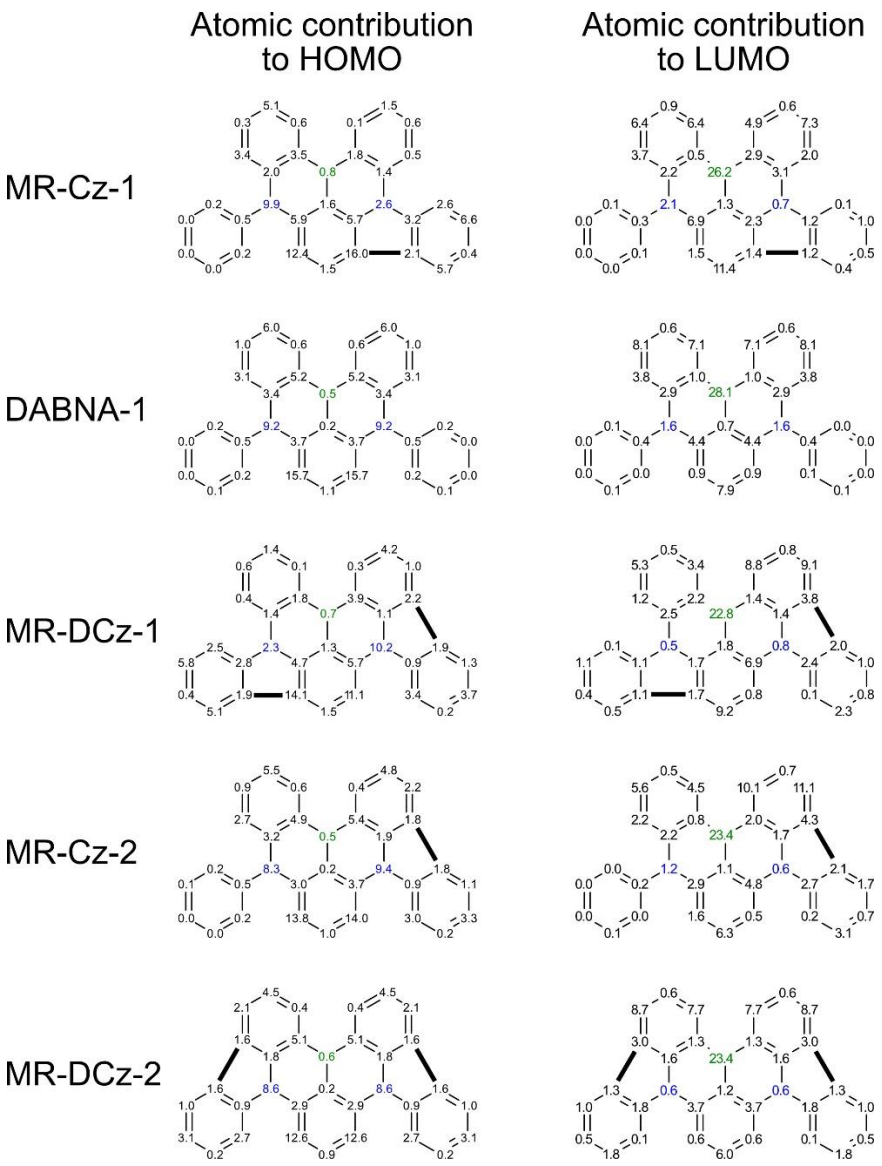

Figure S39. Percentage atomic contributions to the HOMO and LUMO of five model MR-TADF isomers, obtained from Mulliken-partition analysis at the Hartree-Fock/def2-TZVP level of theory. Blue/green/black-colored numbers indicate nitrogen/boron/carbon atoms and solid bold bonds highlight the additional C–C connectivity.

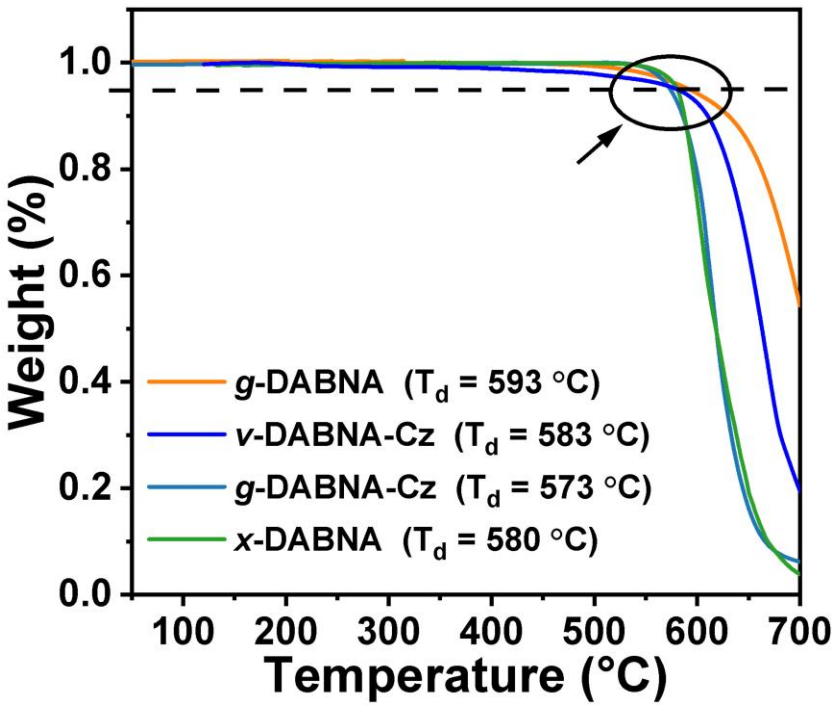

Figure S40. TGA curves of *g*-DABNA, *v*-DABNA-Cz, *v*-DABNA-Cz and *x*-DABNA at a scanning rate of 10 ^{o}C min^{-1} under N_2.

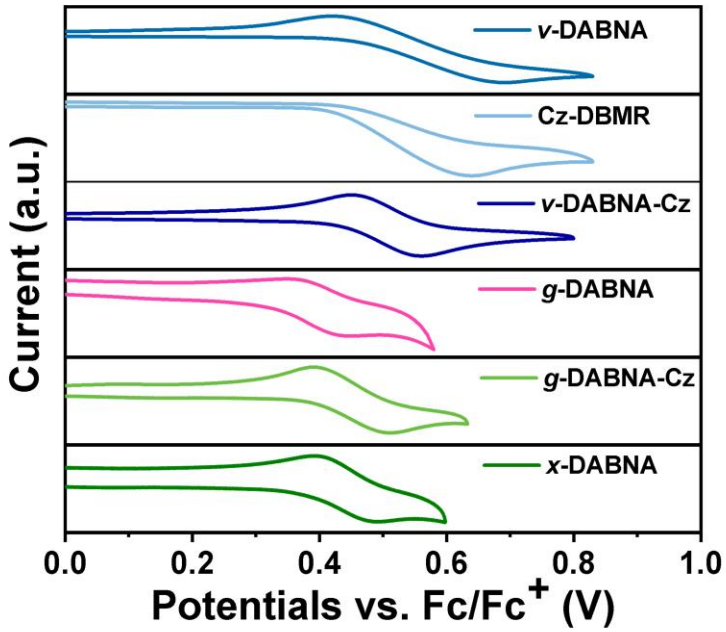

Figure S41. CV curves of *v*-DABNA, Cz-DBMR, *v*-DABNA-Cz, *g*-DABNA, *v*-DABNA-Cz and *x*-DABNA.

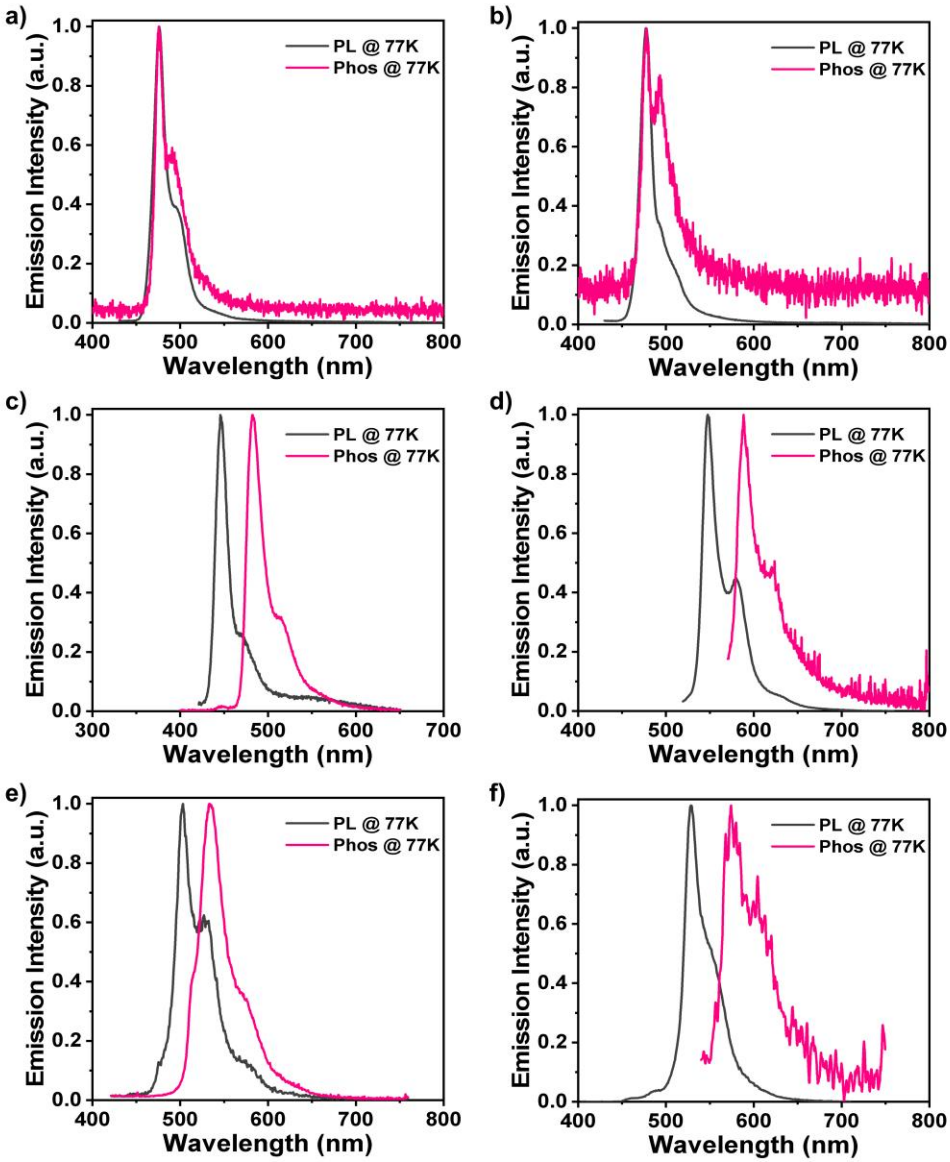

Figure S42. Fluorescence and phosphorescence spectra of a) *v*-DABNA, b) Cz-DBMR, c) *v*-DABNA-Cz, d) *g*-DABNA, e) *v*-DABNA-Cz and f) *x*-DABNA.

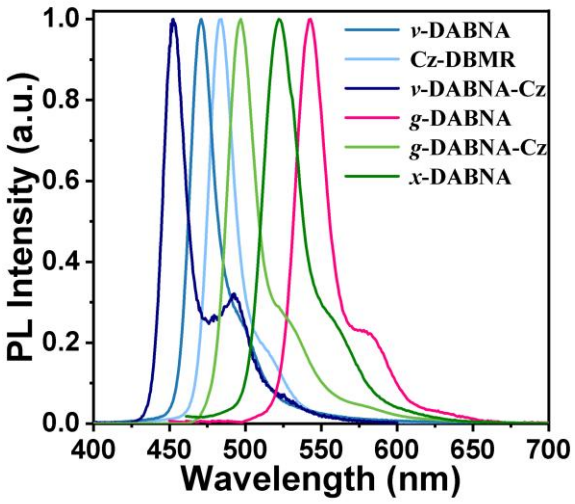

Figure S43. PL spectra of 1 wt% *v*-DABNA, CzDBMR, *v*-DABNA-Cz, *g*-DABNA, *v*-DABNA-Cz and *x*-DABNA: PhCzBCz doped films.

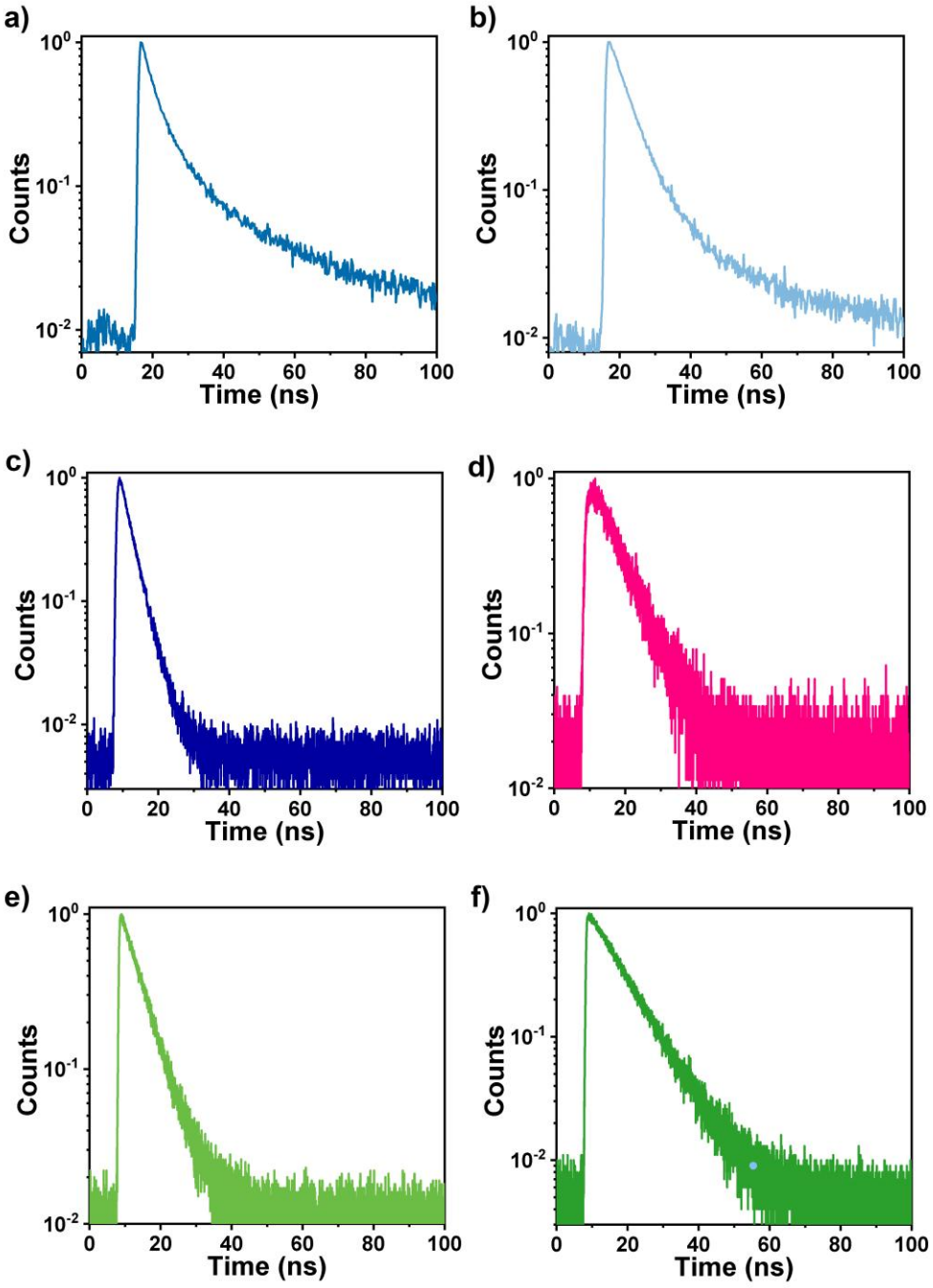

Figure S44. Transient fluorescence decay curves of 1 wt% a) *v*-DABNA, b) Cz-DBMR, c) *v*-DABNA-Cz, d) *g*-DABNA, e) *v*-DABNA-Cz and f) *x*-DABNA: PhCzBCz doped films.

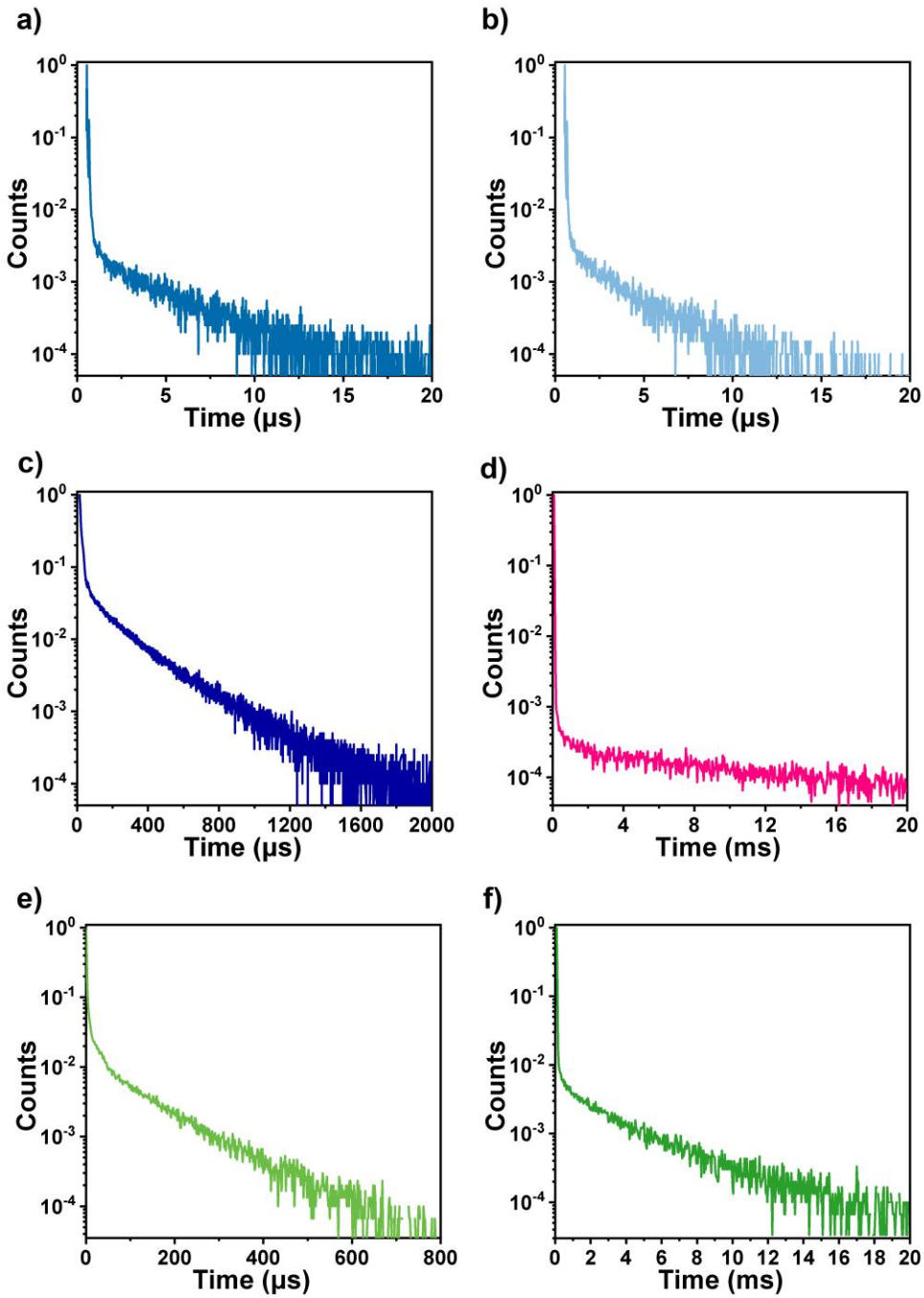

Figure S45. Delayed fluorescence decay curves of 1 wt% a) *v*-DABNA, b) Cz-DBMR, c) *v*-DABNA-Cz, d) *g*-DABNA, e) *v*-DABNA-Cz and f) *x*-DABNA: PhCzBCz doped films.

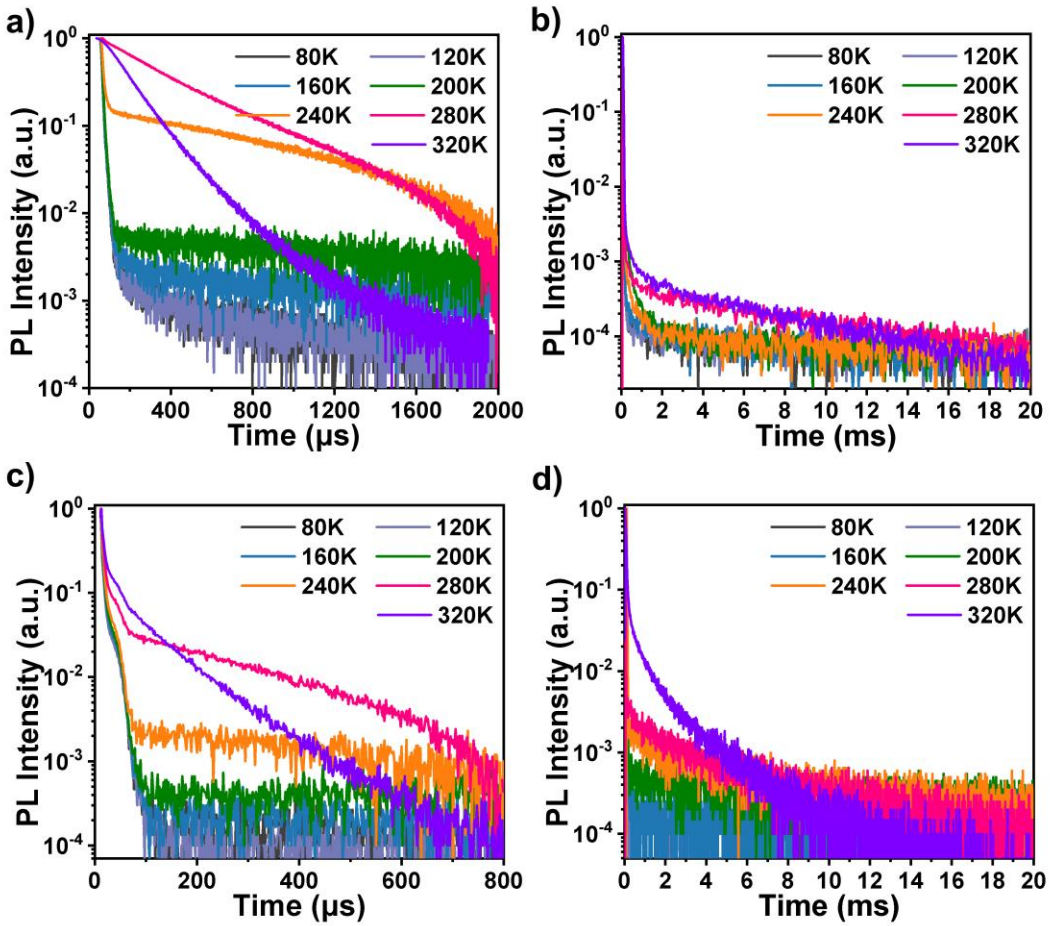

Figure S46. Transition PL decay curves of 1 wt% a) *v*-DABNA-Cz, b) *g*-DABNA, c) *v*-DABNA-Cz and d) *x*-DABNA: PhCzBCz doped films under different temperatures from 80 to 320 K.

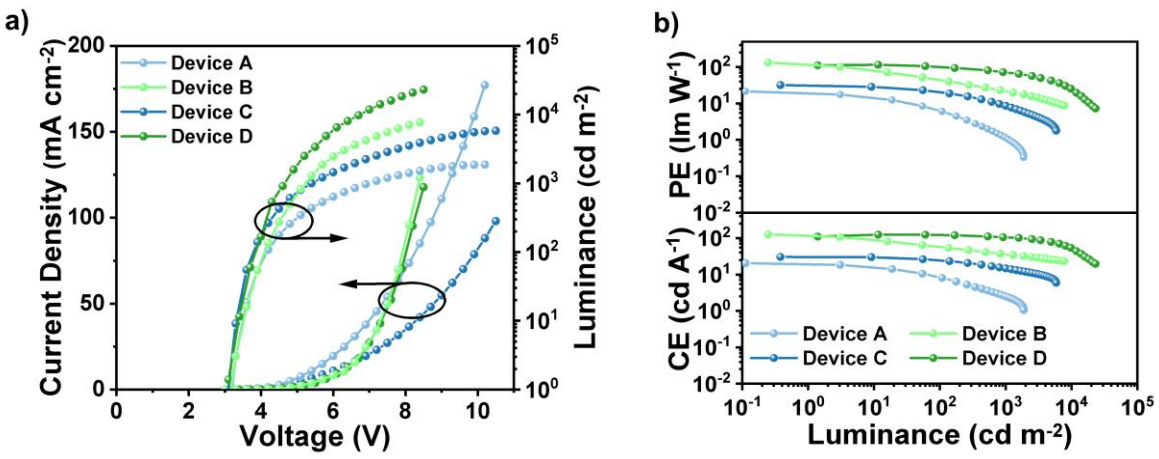

Figure S47. EL characteristics of *v*-DABNA-Cz and *x*-DABNA. a) *J*-*V*-*L* curves. b) CE-*L* and PE-*L* curves.

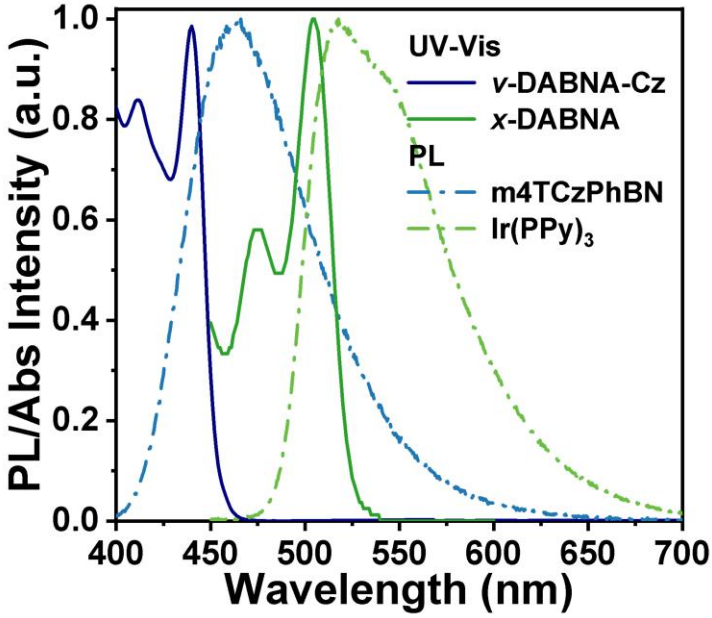

Figure S48. UV–vis absorption spectra of *v*-DABNA-Cz and *x*-DABNA in toluene at a concentration of 10^{-5} M as well as PL spectra of 20 wt% $Ir(ppy)_3$ and m4TCzPhBN: PhCzBCz doped films.

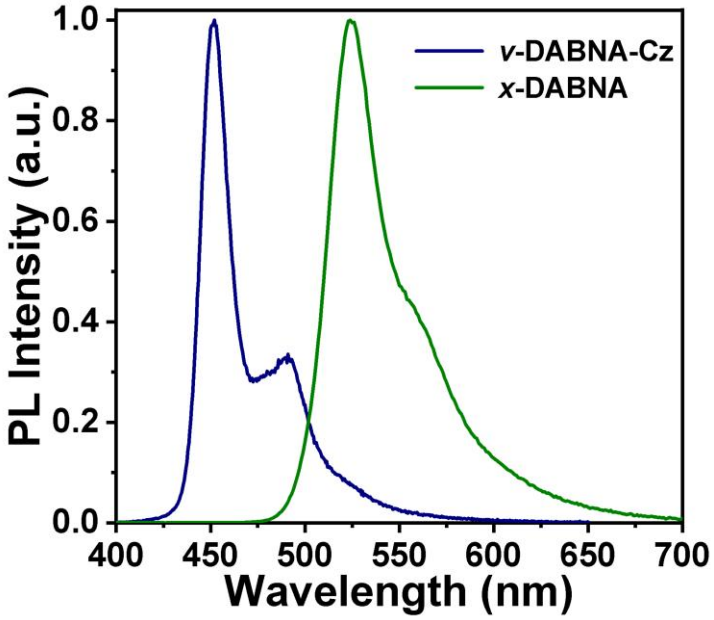

Figure S49. PL spectra of *v*-DABNA-Cz and *x*-DABNA: PhCzBCz ternary sensitized films.

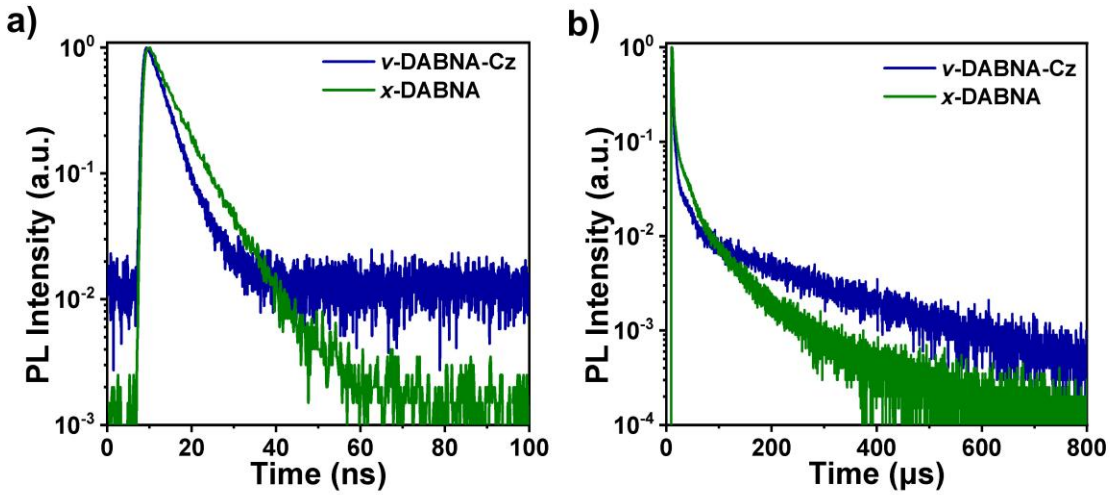

Figure S50. Transient PL decay spectrua of *v*-DABNA-Cz and *x*-DABNA: PhCzBCz ternary sensitized films.

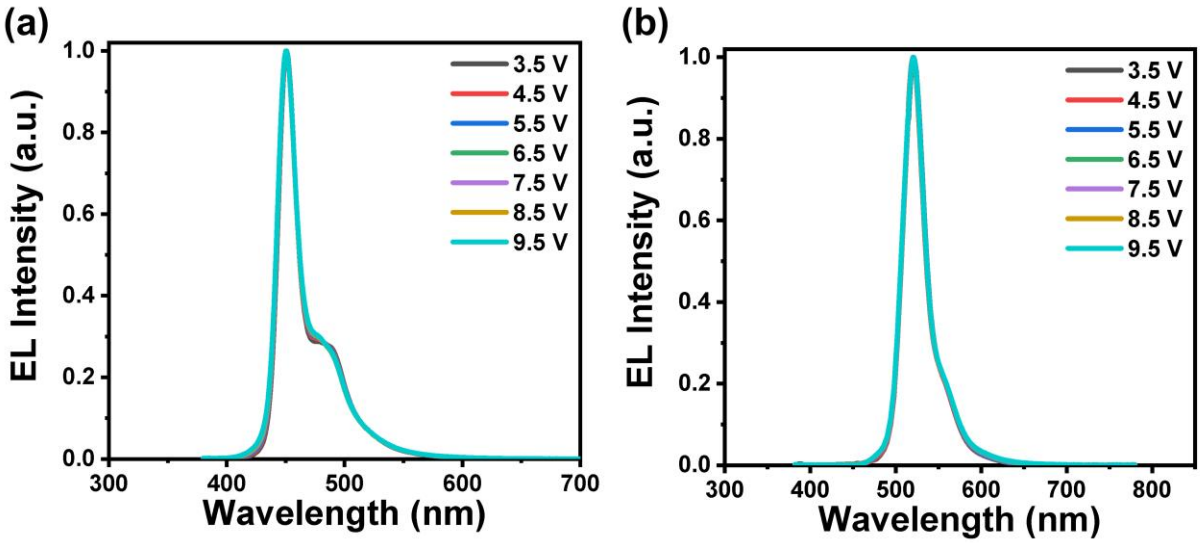

Figure S51. The normalized EL spectra operated at different voltages of a) *v*-DABNA-Cz and b) *x*-DABNA-based devices with sensitizers.

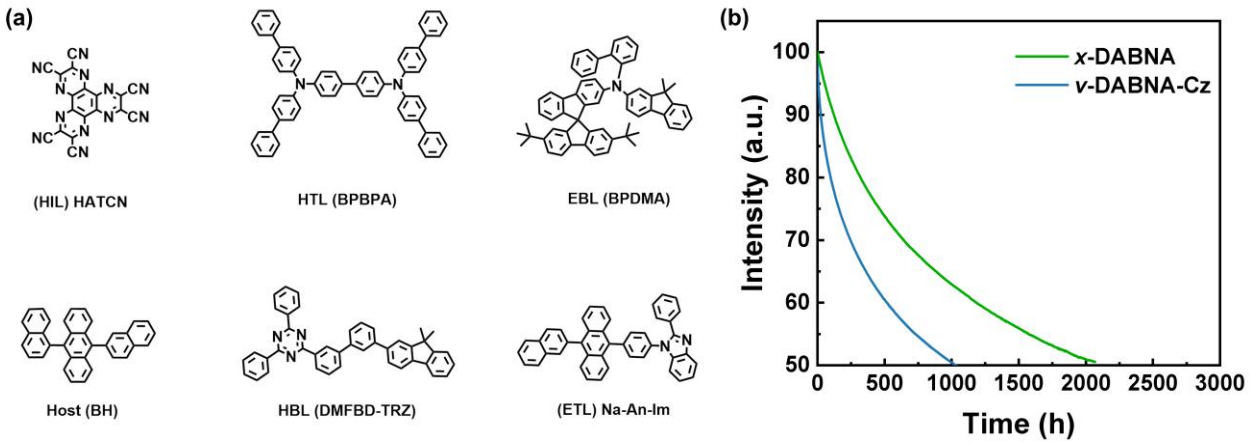

Figure S52. a) Chemical structure of materials used in the devices. (The device configuration: [ITO/HATCN (10 nm)/HTL (30 nm)/EBL (10 nm)/BH: 25 % sensitizers: 1 wt% emitters (25 nm)/HBL (10 nm)/ETL (35 nm)/Liq (2 nm)/Al (100 nm)]) b) Lifetime curve of *v*-DABNA-Cz and *x*-DABNA-based devices at initial luminance of 1000 cd m^{-2}. (The operational lifetime measured at an initial current density of 10 mA cm^{-2}, and operational lifetime at an initial luminance of 1000 cd m^{-2} calculated by adopting a degradation acceleration factor that relates luminance to lifetime, *viz*. $\mathrm{LT}(1000\ \mathrm{cd\ m^{-2}}) = \mathrm{LT}(L_0) \times \left[\frac{L_0}{1000\ \mathrm{cd\ m^{-2}}}\right]^n$ with n = 1.7.).

7. Supplementary Tables

Table S1. Summary of the EL data of mode compounds-based devices.

Device	λ_{em}[a)] [nm]	FWHM[b)] [nm/eV]	V_{on}[c)] [V]	L_{max}[d)] [cd m^{-2}]	CE_{max}[e)] [cd A^{-1}]	PE_{max}[f)] [lm W^{-1}]	EQE[g)] [%]	CIE[h)] (x, y)
MR-Cz-1	451	29/0.17	3.2	1460	7.1	6.6	12.5/10.1/6.7	(0.14, 0.05)
DABNA-1	458	25/0.15	3.3	1528	9.6	9.1	16.8/13.4/7.0	(0.14, 0.07)
MR-DCz-1	467	30/0.17	3.2	2041	13.1	11.7	13.1/11.8/6.8	(0.12, 0.13)
MR-Cz-2	471	26/0.15	3.3	2830	18.9	17.5	17.6/16.6/9.7	(0.12, 0.15)
MR-DCz-2	480	30/0.16	3.3	4031	27.9	26.0	17.9/15.2/11.1	(0.10, 0.28)

[a)] EL peak wavelength at 100 cd m^{-2}. [b)] Full width at half maximum of the spectra given in wavelength. [c)] Turn-on voltage at 1 cd m^{-2}. [d)] Maximum luminance. [e)] Maximum current efficiency. [f)] Maximum power efficiency. [g)] Maximum external quantum efficiency, and values at 100 and 1000 cd m^{-2}, respectively. [h)] Value taken at 100 cd m^{-2}.

Table S2. Excited-state properties of model MR-TADF molecules calculated at the CIS and CC levels of theory. f_{S1} denotes the oscillator strength of the S_1 state. All values are given in eV.

Emitter	E_{S1} [Exp]	E_{S1} [CIS]	E_{S1} [CC]	E_{T1} [CC]	ΔE_{S1T1} [CC]	f_{S1} [CC]	E_{S1} [Corr]
MR-Cz-1	2.88	4.53	2.97	2.61	0.36	0.34	–1.57
DABNA-1	2.82	4.61	2.94	2.75	0.19	0.30	–1.67
MR-DCz-1	2.76	4.42	2.86	2.56	0.30	0.54	–1.55
MR-Cz-2	2.74	4.50	2.86	2.63	0.24	0.42	–1.64
MR-DCz-2	2.69	4.44	2.81	2.62	0.19	0.51	–1.63

Table S3. Excited-state properties of model MR-TADF molecules obtained experimentally and calculated at the B3LYP level of theory. All values are given in eV.

Emitter	E_{S1} [Exp]	E_{T1} [Exp]	ΔE_{S1T1} [Exp]	E_{S1} [TD]	ΔE_{T1} [TD]	ΔE_{S1T1} [TD]
MR-Cz-1	2.88	2.63	0.25	3.14	2.61	0.53
DABNA-1	2.82	2.63	0.19	3.14	2.65	0.49
MR-DCz-1	2.76	2.55	0.21	2.99	2.53	0.46
MR-Cz-2	2.74	2.60	0.16	3.02	2.55	0.47
MR-DCz-2	2.69	2.56	0.14	2.93	2.52	0.41

Table S4. One- and two-electron integrals for model MR-TADF molecules, along with the corresponding S_1 energies obtained from integrals alone (E_{S1}[Ints]) and from the combined contributions of integrals and electron correlation effect (E_{S1}[Ints+Corr]). All values are given in eV.

Emitter	h_{HH}	h_{LL}	J_{HH}	J_{HL}	K_{HL}	E_{S1} [Ints]	E_{S1} [Ints+Corr]
MR-Cz-1	-12.01	-6.11	4.99	4.05	0.38	5.33	3.77
DABNA-1	-12.03	-6.19	5.08	4.22	0.36	5.35	3.68
MR-DCz-1	-11.86	-6.20	4.66	3.83	0.31	5.15	3.59
MR-Cz-2	-11.86	-6.18	4.73	3.97	0.30	5.22	3.58
MR-DCz-2	-11.72	-6.19	4.44	3.79	0.26	5.14	3.51

Table S5. Summary of the physical properties of derived compounds.

Emitter	λ_{abs}[a] [nm]	λ_{em}[b] [nm]	FWHM[c] [nm/eV]	E_{S1}[d] [eV]	E_{T1}[e] [eV]	ΔE_{ST}[f] [eV]	E_g[g] [eV]	HOMO[h] [eV]	LUMO[i] [eV]	Φ_{PL}[j] [%]
v-DABNA	457	466	16/0.09	2.69	2.65	0.04	2.64	-5.24	-2.60	94
Cz-DBMR	468	477	16/0.09	2.67	2.65	0.02	2.56	-5.22	-2.66	93
v-DABNA-Cz	440	448	16/0.10	2.86	2.64	0.22	2.94	-5.23	-2.29	96
g-DABNA	529	539	23/0.10	2.33	2.14	0.19	2.27	-5.12	-2.85	95
g-DABNA-Cz	484	495	21/0.10	2.55	2.41	0.14	2.46	-5.19	-2.73	93
x-DABNA	504	520	24/0.11	2.42	2.25	0.17	2.37	-5.17	2.80	93

[a] Peak wavelength of the lowest energy absorption band. [b] Peak wavelength of the PL spectrum in toluene (1×10^{-5} M, 298 K). [c] Full width at half maximum of the spectra given in wavelength. [d] Singlet energy estimated from the onset of the fluorescence spectrum in toluene (10^{-5} M, 77 K). [e] Triplet energy estimated from the onset of the phosphorescence spectrum in a frozen toluene matrix (10^{-5} M, 77 K). [f] $\Delta E_{ST} = E_{S1} - E_{T1}$. [g] Optical band gap estimated from the absorption edge of the UV–vis spectrum. [h] Determined from cyclic voltammetry using the formula: $E_{HOMO} = -(E_{ox} + 4.8)$ eV. [i] Determined from the formula: $E_{LUMO} = E_{HOMO} + E_g$. [j] Absolute photoluminescence quantum yield measured with an integral-sphere system in N_2-bubbling toluene.

Table S6. Summary of photophysical data of 1 wt % derived compounds: PhCzBCz doped films.

Emitter	λ_{em}[a] [nm]	FWHM[b] [nm/eV]	Φ_{PL}[c] [%]	Φ_F[d] [%]	Φ_{TADF}[e] [%]	τ_F[f] [ns]	τ_{TADF}[g] [μs]	k_r[h] [10^7 s^{-1}]	k_{nr}[i] [10^6 s^{-1}]	k_{ISC}[j] [10^7 s^{-1}]	k_{RISC}[k] [10^4 s^{-1}]
v-DABNA	470	19/0.10	97	58.0	39.0	8.6	3.0	6.7	2.1	4.7	56.6
Cz-DBMR	484	19/0.11	98	43.8	44.2	7.2	2.5	6.1	1.2	7.7	73.2
v-DABNA-Cz	452	18/0.11	97	43.9	53.1	3.3	234.2	13.0	6.8	16.6	1.0
g-DABNA	542	27/0.10	96	90.0	6.0	7.2	2950.1	12.6	6.7	5.8	0.5
g-DABNA-Cz	497	23/0.11	96	52.1	43.9	7.4	82.3	6.8	4.4	6.2	21.3
x-DABNA	521	28/0.12	97	72.5	24.5	8.7	1392.4	8.2	2.5	3.0	0.9

[a] PL emission maximum. [b] Full width at half maximum of the PL spectrum. [c] The total photoluminescence quantum yield (Φ_{PL}). [d] The prompt fluorescent (Φ_F) component of Φ_{PL}. [e] The delayed fluorescent (Φ_{TADF}) component of Φ_{PL}. [f] The lifetime of prompt fluorescence (τ_F). [g] The lifetime of delayed fluorescence (τ_{TADF}). [h] The rate constant of radiative decay (k_r). [i] The rate constant of non-radiative decay (k_{nr}). [j] The rate constant of intersystem crossing (k_{ISC}). [k] The rate constant of reverse intersystem crossing (k_{RISC}).

Table S7. Summary of photophysical data of 1 wt % *v*-DABNA-Cz and *x*-DABNA: PhCzBCz doped films with sensitizer.

Emitter	λ_{em}[a] [nm]	FWHM[b] [nm/eV]	Φ_{PL}[c] [%]	Φ_F[d] [%]	Φ_{TADF}[e] [%]	τ_F[f] [ns]	τ_{TADF}[g] [μs]	k_r[h] [10^7 s^{-1}]	k_{nr}[i] [10^6 s^{-1}]	k_{ISC}[j] [10^7 s^{-1}]	k_{RISC}[k] [10^4 s^{-1}]
v-DABNA-Cz	452	18/0.11	98	41.5	56.5	4.2	100.1	9.9	2.2	13.7	2.4
x-DABNA	523	29/0.12	98	37.2	60.8	8.2	48.4	4.5	0.9	7.6	54.0

[a] PL emission maximum. [b] Full width at half maximum of the PL spectrum. [c] The total photoluminescence quantum yield (Φ_{PL}). [d] The prompt fluorescent (Φ_F) component of Φ_{PL}. [e] The delayed fluorescent (Φ_{TADF}) component of Φ_{PL}. [f] The lifetime of prompt fluorescence (τ_F). [g] The lifetime of delayed fluorescence (τ_{TADF}). [h] The rate constant of radiative decay (k_r). [i] The rate constant of non-radiative decay (k_{nr}). [j] The rate constant of intersystem crossing (k_{ISC}). [k] The rate constant of reverse intersystem crossing (k_{RISC}).

8. References

[S1] M. J. Frisch, G. W. Trucks, H. B. Schlegel, G. E. Scuseria, M. A. Robb, J. R. Cheeseman, G. Scalmani, V. Barone, B. Mennucci, G. A. Petersson, H. Nakatsuji, M. Caricato, X. Li, H. P. Hratchian, A. F. Izmaylov, J. Bloino, G. Zheng, J. L. Sonnenberg, M. Hada, M. Ehara, K. Toyota, R. Fukuda, J. Hasegawa, M. Ishida, T. Nakajima, Y. Honda, O. Kitao, H. Nakai, T. Vreven, J. A. Montgomery, Jr., J. E. Peralta, F. Ogliaro, M. Bearpark, J. J. Heyd, E. Brothers, K. N. Kudin, V. N. Staroverov, T. Keith, R. Kobayashi, J. Normand, K. Raghavachari, A. Rendell, J. C. Burant, S. S. Iyengar, J. Tomasi, M. Cossi, N. Rega, J. M. Millam, M. Klene, J. E. Knox, J. B. Cross, V. Bakken, C. Adamo, J. Jaramillo, R. Gomperts, R. E. Stratmann, O. Yazyev, A. J. Austin, R. Cammi, C. Pomelli, J. W. Ochterski, R. L. Martin, K. Morokuma, V. Zakrzewski, G. A. Voth, P. Salvador, J. J. Dannenberg, S. Dapprich, A. D. Daniels, O. Farkas, J. B. Foresman, J. V. Ortiz, J. Cioslowski, and D. J. Fox, Gaussian, Inc., Wallingford CT, **2013**.

[S2] Q. Sun, X. Zhang, S. Banerjee, P. Bao, M. Barbry, N. S. Blunt, N. A. Bogdanov, G. H. Booth, J. Chen, Z.-H. Cui et al., *J. Chem. Phys.*, 2020, **153**, 024109.

[S3] F. Neese, F. Wennmohs, U. Becker, C. Riplinger, *J. Chem. Phys.*, 2020, **152**, 224108.

[S4] T. Lu, F. Chen, *J. Comput. Chem.*, 2012, **33**, 580-592.

[S5] A. Szabó, & N. S. Ostlund, (**1982**). Modern quantum chemistry : introduction to advanced electronic structure theory.

[S6] Q. Zhang, H. Kuwabara, W. J. Potscavage, S. Huang, Y. Hatae, T. Shibata, C. Adachi, *J. Am. Chem. Soc.*, 2014, **136**, 18070.

[S7] Q. Zhang, B. Li, S. Huang, H. Nomura, H. Tanaka, C. Adachi, *Nat. Photonics*, 2014, **8**, 326.

[S8] T.-L. Wu, M.-J. Huang, C.-C. Lin, P.-Y. Huang, T.-Y. Chou, R.-W. Chen-Cheng, H.-W. Lin, R.-S. Liu, C.-H. Cheng, *Nat. Photonics*, 2018, **12**, 235.